ABSTRACT

WANG, ZHAOHUI. A Robin Robin Domain Decomposition Method for a Stokes-Darcy System with a Locally Modified Mesh. (Under the direction of Dr. Zhilin Li.)

The coupled system of Stokes-Darcy arises in many applications of mathematical modeling, such as petroleum extraction, ground/underground water conduits and karst aquifers. In this system, the fluid flow is modeled by the Stokes equations, while the porous media flow is modeled by the Darcy's law. However, one challenge we encountered in this problem is obtaining accurate and efficient numerical solutions.

In this dissertation, we first propose a new numerical method for solving this coupled system. The method is based on a Robin-Robin domain decomposition method with a locally modified Cartesian mesh. The Robin-Robin domain decomposition method (Robin-Robin DDM) provides a way to solve this system numerically. One key step is to convert the coupled equations into separate ones. Next, for a complicated geometric structure, it is expensive and difficult to build a body fitted mesh which is required by Robin-Robin DDM. Thus the method of locally modified mesh addresses this issue and provides simplicity in building a mesh and efficiency in reducing computational cost. Moreover, two types of interface conditions are considered and numerically tested.

Another numerical method we proposed is based on an augmented variable method. This method accurately computes the gradient near the boundary or the interface. It is tested on a Poisson equation with a circular interface. Our result shows that an improved accuracy of the gradient is obtained in comparison with standard approaches.

A Robin Robin Domain Decomposition Method for a Stokes-Darcy System with a Locally Modified Mesh

by
Zhaohui Wang

A dissertation submitted to the Graduate Faculty of
North Carolina State University
in partial fulfillment of the
requirements for the Degree of
Doctor of Philosophy

Applied Mathematics

Raleigh, North Carolina

2016

APPROVED BY:

Dr. Kazufumi Ito	Dr. Xiaobiao Lin
Dr. Hua Zhou	Dr. Donald Martin

Dr. Zhilin Li
Chair of Advisory Committee

DEDICATION

To my parents and wife.

Xin Wang, Wenping Liu, Shihui Jiao

for their endless love and support.

BIOGRAPHY

Zhaohui Wang was born in the city of Shenyang, China in 1986. He developed interest into science during his early age. He studied in NO.20 high school of Shenyang from 2004 to 2006. In 2006, he enrolled in University of Science and Technology Beijing, where he received his Bachelor degree of Mathematics and Computer Science. In 2009, he was selected into a 3+1+1 program between University of Dundee and University of Science and Technology Beijing. At that time, he established an interest into applied mathematics. In 2011, he came to US and studied applied mathematics at North Carolina State University. He started to do research in numerical analysis and scientific computing under the direction of Dr. Zhilin Li. Meanwhile, he received his Master degree in Statistics in 2014. Zhaohui enjoys applying quantitative knowledge to application problems. He has accepted a full time position at Wells Fargo.

ACKNOWLEDGEMENTS

I would like to express my deepest gratitude to my advisor, Dr. Zhilin Li for his guidance and support throughout my PhD study. I learned so much from him, not only from the inspiring discussions and insightful advises, but from the right attitude towards research and life. His wisdom, enthusiasm and patience helped me to accomplish this wonderful journey, which is valuable for my life.

I would also like to thank my committee members, Dr. Kazufumi Ito, Dr. Xiaobiao Lin, Dr. Hua Zhou and Dr. Donald Martin for reviewing my dissertation and offering valuable suggestions. Thanks to Mrs. Denise Seabrooks and Mrs. Lesa Denning for their help during my five years in applied mathematics program.

Thanks also go to my dear friends in NC State University for their help and collaboration on my study: Sidong Zhang, Guanyu Chen, Peng Song, Gadi Elamami, Ranya Ali, Changjuan Zhang, Xiaofei Peng and Peiqi Huang.

Finally, I want to thank my wife, Shihui Jiao, my parents, Xin Wang and Wenping Liu for their unconditional support and love that keep me moving forward.

TABLE OF CONTENTS

LIST OF TABLES

LIST OF FIGURES

Chapter 1

Introduction

.

1.1 Interface Problems

1.1.1 Background of Interface Problems

Interface problems constitute a major component of mathematical modeling and arise in a wide range of applications in science and engineering. For example, the process of fluid flow between soil and surface (see Figure 1.1 as an illustration of the domain and the interface), the development simulation of crystal growth and moving fronts, heat conduction in materials with different conductivities, or bubble motion between fluid and air, see [60] for more applications and discussions. These applications can be modeled by partial differential equations (PDEs) with an interface separating the whole domain into several subdomains. The coefficiens in these PDEs are usually discontinuous across the interface. In many cases even the PDEs are different in each subdomain. As a result, the model be-

comes much more complex and difficult to solve. Standard numerical methods constantly have a poor performance in terms of accuracy and efficiency due to their assumptions of smoothness in solutions and coefficients. Moreover, the proof of existence, uniqueness and stability of solutions in interface problems is considered to be more challenging. In view of these difficulties, we worked on developing numerical algorithms to specifically solve interface problems with the aim to improve accuracy and efficiency of the solutions. In other words, this is the theme of the dissertation.

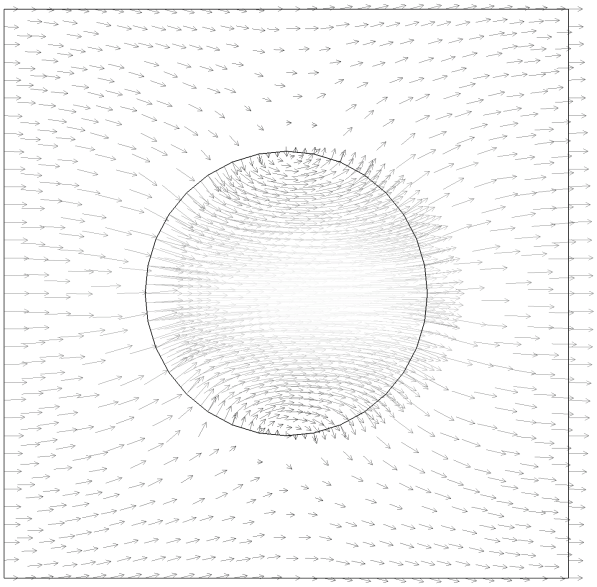

Figure 1.1: A simulation of fluid flow between soil (outside) and surface (inside) separated by the circular interface.

1.1.2 PDEs with Interfaces

A Poisson Equation with an Interface

Consider a Poisson equation on a bounded domain $\Omega \in R^d$ where d is the dimension of the domain.

$$\nabla \cdot (\beta(\mathbf{x})\nabla u(\mathbf{x})) = f(\mathbf{x}), \quad \mathbf{x} \in R^d, \tag{1.1}$$

together with the jump conditions across the interface Γ,

$$[u]_\Gamma = \omega(s), \quad \left[\beta \frac{\partial u}{\partial \mathbf{n}}\right]_\Gamma = \nu(s), \tag{1.2}$$

along with a determined boundary condition on $\partial\Omega$, where $\Gamma \in C^2$ is a smooth interface separating Ω^+ and Ω^-. $\omega(s) \in C^2$ and $\nu(s) \in C^1$ are the two functions defined along the interface Γ. $\mathbf{n}$ is the outward normal direction following the right hand side rule. The interface Γ is usually represented by the level set function $\phi(\mathbf{x})$ at zero. Therefore the two domains are denoted by $\Omega^- = \{\mathbf{x} \in \Omega : \phi(\mathbf{x}) < 0\}$ and $\Omega^+ = \{\mathbf{x} \in \Omega : \phi(\mathbf{x}) > 0\}$. See Figure 1.2 as an example. The coefficient $\beta(\mathbf{x})$ can have a finite discontinuity across the interface Γ, for example,

$$\beta(\mathbf{x}) = \begin{cases} \beta^-(\mathbf{x}) & \text{if } \mathbf{x} \in \Omega^-, \\ \beta^+(\mathbf{x}) & \text{if } \mathbf{x} \in \Omega^+, \end{cases} \tag{1.3}$$

where the jump in β is

$$[\beta]_\Gamma = \lim_{\mathbf{x}\to\Gamma, \mathbf{x}\in\Omega^+} \beta(\mathbf{x}) - \lim_{\mathbf{x}\to\Gamma, \mathbf{x}\in\Omega^-} \beta(\mathbf{x}). \tag{1.4}$$

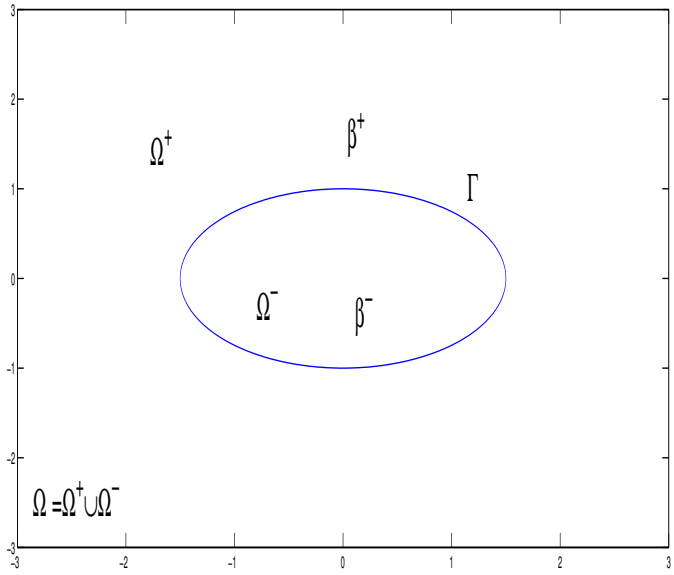

Figure 1.2: A Sketch of rectangular domain $\Omega = \Omega^+ \cup \Omega^-$with an ellipse interface Γ. The cefficients $\beta(x,y)$ have a finite jump across the interface Γ.

The jump conditions along the interface are defined as

$$[u]_\Gamma = u^+(\mathbf{X}(s)) - u^-(\mathbf{X}(s)) = \omega(s), \tag{1.5}$$

$$\left[\beta \frac{\partial u}{\partial \mathbf{n}}\right]_\Gamma = \beta^+(\mathbf{X}(s)) \frac{\partial u^+(\mathbf{X}(s))}{\partial \mathbf{n}} - \beta^-(\mathbf{X}(s)) \frac{\partial u^-(\mathbf{X}(s))}{\partial \mathbf{n}} = \nu(s), \tag{1.6}$$

where $\mathbf{X}(s)$ is a point on Γ and Γ is parameterized by s.

In the case $\omega(s) = 0$, the problem can be written as

$$\nabla \cdot (\beta(\mathbf{x}) \nabla u(\mathbf{x})) = f(\mathbf{x}) + \int_\Gamma \nu(\mathbf{X}(s)) \delta(\mathbf{x} - \mathbf{X}(s)) ds, \quad \mathbf{x} \in R^d. \tag{1.7}$$

The Stokes Equations with Interfaces

Stokes flow, also called creeping flow, simulates the situation where the fluid velocity is slow and viscosity is large [46]. Stokes equations are represented as

$$\begin{cases} -\mu\triangle\mathbf{u}+\nabla p=\mathbf{f}, \\ \nabla\cdot\mathbf{u}=0, \end{cases} \tag{1.8}$$

where $\mathbf{u}$ is fluid velocity, p is the kinematic pressure, μ is fluid viscosity. $\mathbf{f}$ is the body force. Now we consider $\mathbf{f}(\mathbf{X},t)$ is a source strengh of the force defined only on the interface. Similar to the previous case, the interface problem becomes

$$\begin{cases} -\mu\triangle\mathbf{u}+\nabla p=\mathbf{f}+\int_\Gamma \mathbf{f}(\mathbf{X}(s,t))\delta(\mathbf{x}-\mathbf{X}(s,t))ds, \\ \nabla\cdot\mathbf{u}=0. \end{cases} \tag{1.9}$$

1.2 Literature Review

1.2.1 Finite Difference Methods and Finite Element Methods

The partial differential equations (PDEs) we have discussed so far are challenging to solve analytically. In certain situations, the analytical solutions are impossible to obtain. Therefore numerical estimates are highly desired. Finite difference methods provide us with a way to solve differential equations numerically. The 1D case of FD was first developed by L. Euler (1707-1783) and extended by C. Runge (1856-1927) to 2D. The invention of modern computer enlarged the scope of computing and accelerated the development of FD methods. The foundation of FD methods is Taylor expansion, through which the approximation of derivatives and error analysis can be established. By discretizing the differential equa-

tions, a large linear system of equations is built and solved. For more details of FD method, see [51]. A Cartesian mesh is often used in the discretization process of FD method. It is trivial to generate the mesh and the index of grid points is easy to follow and locate. Moreover, there are many well tested packages based on a Cartesian mesh. Those packages are highly optimized in terms of computation time. Besides, they provide numerical solutions with minimal efforts, such as Poisson solver Fishpack [1] and the level set method library (LSMLIB) [22]. One disadvantage of FD method is the difficulty to implement for complicated geometries.

Finite element method (FEM) is first proposed by R. Courant in 1943 and became popular in the 1960s. Compared with FD method, FEM provides better solutions for problems with complicated geometries. Furthermore, it has relatively weaker requirements on regularity. However, one disadvantage of this method is that the mesh generation process can be time consuming. There are many FEM packages available, such as Matlab PDE Tool-Box and Freefem++ [36].

1.2.2 The Stokes Equations

The Stokes equations, also called the Stokes flow or creeping flow, are a type of fluid flow with low advective effects and high viscous effects [46]. In other words, the Reynolds number is low and less than 1. Stokes equations describe a number of physical scenarios, such as weather evolvement, ocean movement, water flow within a pipe, even the design of planes. Moreover, the Stokes equations are a linearization of the Navier-Stokes equations. A few highly optimized solvers are available [54, 91, 48, 32]. We will discuss the formulation of the Stokes equations in the following chapter.

1.2.3 The Darcy's Law

Darcy's law, also called Newton's second law, was first proposed by Henry Darcy from the derivation of the Navier-Stokes equations [23]. It models the fluid flow through porous medium, such as the flow in aquifers and conduits, water penetrating into sand bed. This system laid the foundation for hydrogeology and is widely used by mathematicians, physicists and geologists [31, 47]. We will introduce this system with more details in the next chapter.

1.2.4 The Stokes-Darcy System

The coupled system of Stokes equations and the Darcy's law arises in many applications of mathematical modeling. For example, this system models the physical process of flows across interfaces between soil and surface, petroleum extraction in vuggy porous medium, heat transfer between fibrous insulation and surface flow in Karst aquifers. Moreover, it has been widely applied in biology and medical science, such as the blood motion in human lungs, solid tumors and vessels, personalized medicine and bio-medicine. In this system, the fluid flow is described by the Stokes equations, while the porous medium flow is modeled by the Darcy's law. Although individually, the equations for the Stokes-Darcy flows are straightforward and well established, when these two PDE systems are coupled across an interface, there are challenges. The interface conditions between these two systems are the key part. Several conditions have been proposed [74, 82, 6]. In this dissertation, we consider the well accepted Beavers-Joseph-Saffman (BJS) [74, 82, 44] interface conditions and Beavers-Joseph(BJ) interface conditions. For this dissertation, we investigate both the two types conditions.

Consider the coupled Stokes-Darcy system on a bounded domain $\Omega_p \cup \Omega_f \in \mathbf{R}^d$. The

motion of the fluid in Ω_f is modeled by the Stokes equations

$$-\nabla \cdot \mathbf{T}(\mathbf{u}_f, p_f) = \mathbf{f}, \tag{1.10}$$

$$\nabla \cdot \mathbf{u}_f = 0, \tag{1.11}$$

where $\mathbf{u}_f$ is the fluid velocity, p_f is the kinematic pressure, and $\mathbf{f}$ is the body force. $\mathbf{T}(\mathbf{u}_f, p_f) = 2\nu\mathbf{D}(\mathbf{u}_f) - p_f\mathbf{I}$ is the stress tensor and $\mathbf{D}(\mathbf{u}_f) = \frac{1}{2}(\nabla\mathbf{u}_f + \nabla^T\mathbf{u}_f)$ is the strain rate tensor. ∇ and $\nabla\cdot$ represent gradient operator and divergence operator respectively. The parameter $\nu > 0$ in the stress tensor is the kinematic viscosity of the fluid.

In the porous media region Ω_p, the fluid motion is modeled by Darcy's law

$$\mathbf{u}_p = -\mathbf{K}\nabla\phi_p, \tag{1.12}$$

$$\nabla \cdot \mathbf{u}_p = 0, \tag{1.13}$$

where $\mathbf{u}_p$ is the fluid velocity, $\mathbf{K}$ is the hydraulic conductivity tensor, and ϕ_p is the hydraulic head.

On $\Gamma = \Omega_f \cap \Omega_p$, let $\mathbf{n}_f$ denote the unit outward normal vector from Ω_f at Γ and $\mathbf{n}_p$ denote outward normal vector from Ω_p at Γ. τ_j $(j = 1, ..., d-1)$ represents unit tangential vectors on Γ following right hand rule. See Figure 1.3 as an example of the domain. Along the interface Γ, if we assume the nondimensional porosity of the Darcy region is 1, we have the mass conservation condition across Γ:

$$\mathbf{u}_f \cdot \mathbf{n}_f = -\mathbf{u}_p \cdot \mathbf{n}_p. \tag{1.14}$$

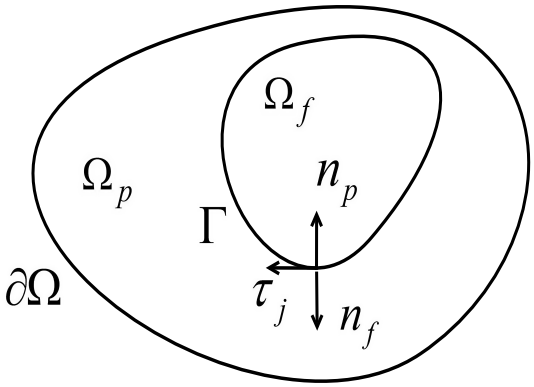

Figure 1.3: Sketch of a free flow region Ω_f, a porous media region Ω_p, and the interface Γ, the normal direction n_f and tangential direction τ_j, as well as boundary $\partial\Omega$.

The second interface condition is the balance of normal stress across Γ:

$$-\mathbf{n}_f \cdot (\mathbf{T}(\mathbf{u}_f, p_f) \cdot \mathbf{n}_f) = g\phi_p, \tag{1.15}$$

where g is the acceleration parameter. As the fluid is viscous, a condition for tangential fluid velocity is needed [49]. A simple assumption is free slippage along Γ, $\tau_j \cdot \mathbf{u}_f = 0$. But in [6], it is shown that boundary condition agrees with experimental evidence when slip of velocity is proportional to shear stress along Γ. This leads to the full Beavers-Joseph interface condition:

$$\tau_j \cdot (\mathbf{u}_f - \mathbf{u}_p) = \frac{\sqrt{\tilde{k}_j}}{\nu\alpha_1}(-\tau_j \cdot (\mathbf{T}(\mathbf{u}_f, p_f) \cdot \mathbf{n}_f)), \tag{1.16}$$

where $\tilde{k}_j = \tau_j \cdot \nu\mathbf{K} \cdot \tau_j$, and α_1 is some constant. It turns out that the term $\tau_j \cdot \mathbf{u}_p$ is much smaller compared with other terms [6]. In this way we can get the simplified BJS interface condition [82, 44] which is derived from a statistical approach:

$$-\tau_j \cdot (\mathbf{T}(\mathbf{u}_f, p_f) \cdot \mathbf{n}_f) = \alpha\tau_j \cdot \mathbf{u}_f. \tag{1.17}$$

These interface conditions ensure the continuity of velocity and stress in the normal direction across the interface, but the pressure can be discontinuous [30].

1.2.5 Numerical Methods for Interface Problems

The coupled Stokes-Darcy System is a type of interface problem. It consists of two independent equation systems, i.e., the Stokes equations and the Darcy's law. The two equations are combined by interfaces. In comparison, the Poisson interface problem we discussed above consists of a single equation with a parameter discontinuity across the interface. Next, we review numerical methods which have been applied to solve both these two types of interface problem.

Numerical Methods for Interface Problems with a Single System

First, Immersed boundary (IB) method is first introduced by Peskin [76, 77, 78, 73] to solve interface problems. The idea of immersed boundary (IB) method is to decompose a singular source to nearby grid points by using discrete delta functions. This method lacks accuracy in the infinity norm.

Secondly, the immersed interface method (IIM). It was first introduced in 1994 by Z. Li and R. LeVeque [52, 57] for interface problems such as elliptic equations with singular source terms and discontinuous coefficients. IIM not only provides desired order of accuracy, but also minimizes the computational cost. Reserch results have shown that IIM provides second order accuracy in L^{∞} norm which is an improvement compared with IB method [5, 40, 59]. A number of interface problems have been solved by IIM, such as interface problems with parabolic equation [55], Stokes equations [53, 61, 63], Navier-Stokes equatiosn [42, 62]. For moving interface problems [56], Hele-Shaw problems [38], crystal

growth [87], three dimensional problems [24, 90], inverse interface problems [41], electro migration of voids [66], interfacial flows [95], and adaptive mesh refinement for interface problems [65, 64]. We refer readers to [60] for more details.

In spite of the methods we reviewed above, there are other types of methods specifically designed to incorporate with interface problems. The harmonic averaging for discontinuous coefficients method can be used to approximate the jump condition by an integral [7, 85, 88]. This method is capable to provide second order accuracy in the infinity norm in 1D case. But in higher dimensions, the calculation of the integral becomes nontrivial.

Integral equations based on finite difference method is applied to elliptic interface problems [70, 71, 72]. In this method, jump conditions are approximated from the integral equation. This method shows a second order accuracy in the infinity norm in the case of homogeneous source terms. However, for nonhomogeneous source terms, it becomes more complex and nontrivial.

The ghost fluid method (GFM) is developed for elliptic interface problems [67, 68]. It follows the idea of IIM and builds finite difference scheme the same way as IIM. However, the way it deals with the jump conditions introduces extra error into the scheme. As a result, GFM presents a first order accuracy in the infinity norm.

Numerical Methods for Interface Problems with a Coupled System

For the coupled Stokes-Darcy system, a number of numerical methods have been developed and trimmed to provide solutions to this coupled system, such as the method of Lagrange multiplier [35, 50], finite element method [3, 16, 19, 45, 81], domain decomposition method [21, 25, 26, 27, 28, 29, 30, 43, 92], DG(discontinuous Galerkin method [34, 80], boundary integral method[89], augmented variable method[58] and two grid method[75].

On the other hand, a number of methods have been constructed for different type of fluid dynamic models, such as Stokes-Brinkman interaction[2, 4, 9, 10, 11, 69, 79, 83, 94, 96]. Those listed methods provide invaluable ideas and tremendous insights for our research. For the domain decomposition method which has been well studied by other researchers. The method based on Dirichlet-Neumann type boundary condition is discussed in [29], but it is shown that the method is sensitive to the choice of the kinematic viscosity ν and the hydraulic conductivity tensor $\mathbf{K}$ [30]. The Robin-Robin type domain decomposition method is proposed in [30, 21, 15]. In [30], the Robin-Robin domain decomposition method has been applied to a simplified BJS interface condition. In [21], the parallel Robin-Robin domain decomposition method is carried out for the BJS interface condition and convergence analysis is presented. In [15], the system with BJ interface condition is analyzed, and both parallel and serial domain decomposition methods are constructed. However, for some complicated domain structures, the mesh generation process might be expensive.

Another similar coupled system of interest is the Stokes-Brinkman interaction. Several methods are developed, such as unified stabilized finite element method [4, 10, 11], Galerkin finite element method [9] and non-conforming finite element method [83, 94, 96].

1.3 Review on Mesh Generation Strategy and Locally Modified Meshes

A key step of applying FEM is to generate a mesh upon which the discretization process can be carried out. One advantage of FEM over FDM is its ability to deal with complex structures and curvatures, see 1.4 as an example.

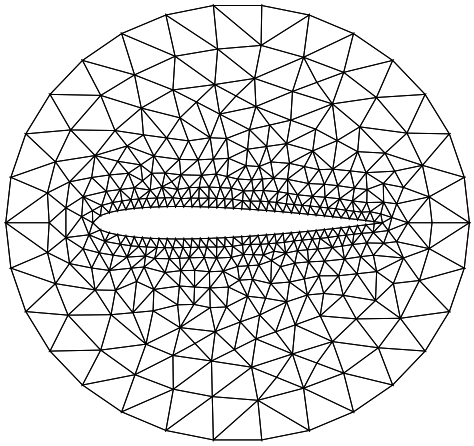

Figure 1.4: A mesh example with complex curvatures and boundaries

The mesh generation process in FEM consists of node and element generation. During the procedure of node generation, many automatic techniques can be used [33, 18, 84]. For example, in the Cavendish method, nodes are first distributed along the boundary with regular intervals. The interior nodes are generated to evenly divide the area into a number of zones. In a zone, the grid of gauge d_i is calculated. If a new node fells into this zone and d_i is great than the current one, the node is rejected. Otherwise, the node is accepted. The next step is element generation process, during which the whole area is covered with elements and no overlap is permitted. The triangulation that maximizes the sum of the smallest angles is constructed to avoid flat elements which may yield poor accuracy. For more details, see [37].

To handle the interface problems directly, we usually use body fitted meshes along with finite element methods. Locally modified mesh method, as one type of body fitted mesh, is a numerical method that disturbs the nodes along the interface. The coefficient matrix is only altered locally [8, 93] by taking advantages of Cartesian meshes. We will discuss this

method further in details in the following chapters.

1.4 Motivations and Outlines

In this dissertation, we focus on solving interface problems, especially the case of the coupled system of Stokes and Darcy equations. One challenge of solving this coupled system is that the two governing PDEs are different in each subdomain, it becomes difficult to solve the system as a whole with desired accuracy. Another challenge is that the mesh generation process is time consuming. To overcome those two challenges, Robin-Robin DDM with a locally modified mesh is investigated. The second motivation is that the gradient of the solution we interested in is constantly one order lower than itself. To address this issue, an augmented variable approach based on finite element method is applied.

In Chapter 2, we focus on the coupled system of Stokes equations and the Darcy's law with BJS interface conditions and BJ interface conditions. A Robin-Robin domain decomposition method is applied to numerically solve this problem and an iterative algorithm is designed to obtain the desired order of accuracy. In order to apply Robin-Robin DDM, a body fitted mesh is required to transfer iterative information between the two models along the interface. In this chapter, we introduce the locally modified mesh method, list the steps to generate the mesh near the interface, select the points to build triangles, and determine regular points and irregular points. Additionally, Robin-Robin DDM with a locally modified mesh and an unstructured mesh are compared.

In Chapter 3, we propose a method to accurately compute the gradient across the interface. Augmented variables are introduced within a small tube near the interface. We show that the accuracy is improved within a Poisson interface problem using this method.

In Chapter 4, we conclude this dissertation by summarizing the ideas and highlights in

our research and point out the potential future directions.

Chapter 2

Robin-Robin Domain Decomposition Method for a Stokes-Darcy System with BJS and BJ interface conditions using a Locally Modified Mesh

.

2.1 Robin-Robin DDM with BJS Interface Conditions

2.1.1 Weak Formulation

In this section, we demonstrate the Robin-Robin DDM [30, 21, 15]. First assume ϕ_p and $\mathbf{u}_f$ are 0 on the boundary $\partial\Omega$ and define the following functional spaces

$$\begin{aligned} H_f &= \{\mathbf{v}_f \in (H^1(\Omega_f))^d | \mathbf{v}_f = 0 \text{ on } \partial\Omega_f \backslash \Gamma\}, && (2.1)\\ Q &= L^2(\Omega_f), && (2.2)\\ H_p &= \{\psi_p \in H^1(\Omega_p) | \psi_p = 0 \text{ on } \partial\Omega_p \backslash \Gamma\}. && (2.3) \end{aligned}$$

The following bilinear forms are defined as

$$\begin{aligned} a_f(\mathbf{u}_f, \mathbf{v}_f) &= 2\nu(\mathbf{D}(\mathbf{u}_f), \mathbf{D}(\mathbf{v}_f)) \quad \text{on } \Omega_f, && (2.4)\\ a_p(\phi_p, \psi_p) &= (\mathbf{K}\nabla\phi_p, \nabla\psi_p) \qquad \text{on } \Omega_p, && (2.5)\\ b_f(\mathbf{v}_f, p_f) &= -(\nabla\cdot\mathbf{v}_f, p_f) \qquad \text{on } \Omega_f. && (2.6) \end{aligned}$$

From [30, 21, 15], the weak formulation of the coupled system becomes: finding $(\mathbf{u}_f, p_f)$ $\in H_f \times Q$, $\phi_p \in H_p$ such that

$$\begin{aligned} &a_f(\mathbf{u}_f, \mathbf{v}_f) + b_f(\mathbf{v}_f, p_f) + g a_p(\phi_p, \psi_p) + \langle g\phi_p, \mathbf{v}_f \cdot \mathbf{n}_f\rangle \\ &-\langle g\mathbf{u}_f \cdot \mathbf{n}_f, \psi_p\rangle + \alpha\langle \mathbf{P}_\tau \mathbf{u}_f, \mathbf{P}_\tau \mathbf{v}_f\rangle = (\mathbf{f}, \mathbf{v}_f) \quad \forall \mathbf{v}_f \in H_f, \psi_p \in H_p, && (2.7)\\ &b_f(\mathbf{u}_f, q_f) = 0 \quad \forall q_f \in Q, && (2.8) \end{aligned}$$

where $(\cdot,\cdot)$ denotes L^2 inner product, $\langle\cdot,\cdot\rangle$ denotes L^2 inner product along the interface Γ, and

$$\mathbf{P}_\tau \mathbf{u}_\mathbf{f} = \sum_{j=1}^{d-1} (\mathbf{u}_f \cdot \tau_j)\tau_j, \tag{2.9}$$

where $\mathbf{P}_\tau$ denotes projection onto tangential space following right hand rule. $\mathbf{v}_f$, q_f and ψ_p are the corresponding test functions.

2.1.2 Robin-Robin DDM with BJS Interface Conditions

Next, we will introduce the Robin-Robin domain decomposition method which is constructed by imposing Robin boundary conditions for the coupled Stokes-Darcy system on the interface. Because Stokes system and Darcy system are well studied and efficient numerical algorithms are thoroughly tested, in light of this, domain decomposition method is utilized to decompose the whole system in order to solve each one individually. We put tildes above some variables to distinguish them from previous notations.

First, let's consider the Robin boundary condition for the Stokes system

$$\mathbf{n}_f \cdot (\mathbf{T}(\tilde{\mathbf{u}}_f, \tilde{p}_f) \cdot \mathbf{n}_f) + \gamma_f \tilde{\mathbf{u}}_f \cdot \mathbf{n}_f = \eta_f \quad \text{on } \Gamma, \tag{2.10}$$

where $\gamma_f > 0$ is a constant, η_f is a function evaluated on Γ. With the boundary condition on Γ, the weak formulation of the Stokes equations becomes: finding $(\tilde{\mathbf{u}}_f, \tilde{p}_f) \in H_f \times Q$, $\eta_f \in L^2(\Gamma)$ such that

$$\begin{aligned} a_f(\tilde{\mathbf{u}}_f, \mathbf{v}_f) + b_f(\mathbf{v}_f, \tilde{p}_f) + \gamma_f \langle \tilde{\mathbf{u}}_f \cdot \mathbf{n}_f, \mathbf{v}_f \cdot \mathbf{n}_f \rangle \\ + \alpha \langle \mathbf{P}_\tau \tilde{\mathbf{u}}_f, \mathbf{P}_\tau \mathbf{v}_f \rangle = (\mathbf{f}, \mathbf{v}_f) + \langle \eta_f, \mathbf{v}_f \cdot \mathbf{n}_f \rangle \quad \forall \mathbf{v}_f \in H_f, \end{aligned} \tag{2.11}$$

$$b_f(\tilde{\mathbf{u}}_f, q_f) = 0 \quad \forall q_f \in Q. \tag{2.12}$$

Next consider the Robin boundary condition for Darcy's law

$$\gamma_p \mathbf{K} \nabla \tilde{\phi}_p \cdot \mathbf{n}_p + g \tilde{\phi}_p = \eta_p \quad \text{on } \Gamma, \tag{2.13}$$

where $\gamma_p > 0$ is a constant and η_p is a function defined similar to η_f unless on Ω_p. The weak formulation of Darcy's law becomes: finding $\tilde{\phi}_p \in H_p$, $\eta_p \in L^2(\Gamma)$ such that

$$\gamma_p a_p(\tilde{\phi}_p, \psi_p) + \langle g \tilde{\phi}_p, \psi_p \rangle = \langle \eta_p, \psi_p \rangle \quad \forall \psi_p \in H_p. \tag{2.14}$$

We combine these weak formulations together. If η_f and η_p are given, there exists a unique solution $(\tilde{\mathbf{u}}_f, \tilde{p}_f) \in H_f \times Q$, $\tilde{\phi}_p \in H_p$ such that

$$\begin{aligned} a_f(\tilde{\mathbf{u}}_f, \mathbf{v}_f) + b_f(\mathbf{v}_f, \tilde{p}_f) + \gamma_f \langle \tilde{\mathbf{u}}_f \cdot \mathbf{n}_f, \mathbf{v}_f \cdot \mathbf{n}_f \rangle + \gamma_p a_p(\tilde{\phi}_p, \psi_p) + \langle g \tilde{\phi}_p, \psi_p \rangle \\ + \alpha \langle \mathbf{P}_\tau \tilde{\mathbf{u}}_f, \mathbf{P}_\tau \mathbf{v}_f \rangle = (\mathbf{f}, \mathbf{v}_f) + \langle \eta_f, \mathbf{v}_f \cdot \mathbf{n}_f \rangle + \langle \eta_p, \psi_p \rangle \quad \forall \mathbf{v}_f \in H_f, \forall \psi_p \in H_p, \end{aligned} \tag{2.15}$$

$$b_f(\tilde{\mathbf{u}}_f, q_f) = 0 \quad \forall q_f \in Q. \tag{2.16}$$

Finally, to determine appropriate values of functions η_f and η_p, we refer back to equations (2.38), (2.39), which are the weak formulations of the Stokes-Darcy system with BJS interface condition. Equations (2.38), (2.39) and (2.15), (2.16) are consistent, i.e., $\mathbf{u}_f = \tilde{\mathbf{u}}_f$, $p_f = \tilde{p}_f$ and $\phi_p = \tilde{\phi}_p$. By subtracting (2.38), (2.39) and (2.15), (2.16), we can get the following equation

$$\begin{aligned} \gamma_f \langle \mathbf{u}_f \cdot \mathbf{n}_f, \mathbf{v}_f \cdot \mathbf{n}_f \rangle + \gamma_p a_p(\phi_p, \psi_p) + \langle g \phi_p, \psi_p \rangle - g a_p(\phi_p, \psi_p) - \langle g \phi_p, \mathbf{v}_f \cdot \mathbf{n}_f \rangle \\ = \langle \eta_f, \mathbf{v}_f \cdot \mathbf{n}_f \rangle + \langle \eta_p, \psi_p \rangle \quad \forall \mathbf{v}_f \in H_f, \forall \psi_p \in H_p. \end{aligned} \tag{2.17}$$

We obtain

$$\begin{aligned} \langle \eta_f - \gamma_f \mathbf{u}_f \cdot \mathbf{n}_f + g\phi_p, \mathbf{v}_f \cdot \mathbf{n}_f \rangle &= 0 \quad \forall \mathbf{v}_f \in H_f, && (2.18) \\ \langle \eta_p - g\phi_p, \psi_p \rangle - (\gamma_p - g) a_p(\phi_p, \psi_p) &= 0 \quad \forall \psi_p \in H_p. && (2.19) \end{aligned}$$

Note that η_p and η_f satisfy

$$\begin{aligned} \eta_f &= \gamma_f \mathbf{u}_f \cdot \mathbf{n}_f - g\phi_p, && (2.20) \\ \eta_p &= \gamma_p' \mathbf{u}_f \cdot \mathbf{n}_f + g\phi_p, && (2.21) \end{aligned}$$

where $\gamma_p' = \gamma_p - g$. We can simply evaluate γ_p' as γ_p without loss of generality and we deduce

$$\begin{aligned} \eta_f &= \gamma_f \mathbf{u}_f \cdot \mathbf{n}_f - g\phi_p, && (2.22) \\ \eta_p &= \gamma_p \mathbf{u}_f \cdot \mathbf{n}_f + g\phi_p. && (2.23) \end{aligned}$$

Therefore, we have the following algorithm of Robin-Robin domain decomposition method [30, 21, 15]:

Step 1: For $k = 1, 2, \ldots$, solve the Stokes system (2.11),(2.12) and the Darcy system (2.14) separately, i.e., finding $(\mathbf{u}_f^k, p_f^k) \in H_f \times Q$, $\phi_p^k \in H_p$ such that

$$\begin{aligned} a_f(\mathbf{u}_f^k, \mathbf{v}_f) + b_f(\mathbf{v}_f, p_f^k) + \gamma_f \langle \mathbf{u}_f^k \cdot \mathbf{n}_f, \mathbf{v}_f \cdot \mathbf{n}_f \rangle + \alpha \langle \mathbf{P}_\tau \mathbf{u}_f^k, \mathbf{P}_\tau \mathbf{v}_f \rangle & && (2.24) \\ = (\mathbf{f}, \mathbf{v}_f) + \langle \eta_f^k, \mathbf{v}_f \cdot \mathbf{n}_f \rangle \quad \forall \mathbf{v}_f \in H_f, & \\ b_f(\mathbf{u}_f^k, q_f) = 0 \quad \forall q_f \in Q, && (2.25) \\ \gamma_p a_p(\phi_p^k, \psi_p) + \langle g\phi_p^k, \psi_p \rangle = \langle \eta_p^k, \psi_p \rangle \quad \forall \psi_p \in H_p. && (2.26) \end{aligned}$$

Step 2: η_f and η_p are updated at each loop as

$$\eta_f^{k+1} = \frac{\gamma_f}{\gamma_p}\eta_p^k + \left(-1 - \frac{\gamma_f}{\gamma_p}\right) g\phi_p^k, \tag{2.27}$$

$$\eta_p^{k+1} = -\eta_f^k + (\gamma_f + \gamma_p)\mathbf{u}_f^k \cdot \mathbf{n}_f. \tag{2.28}$$

Initial values of η_p and η_f are chosen arbitrarily. Conditions (2.27), (2.28) are necessary for the convergence of this algorithm. The algorithm stops when the changes in $\mathbf{u}_f$, p_f and ϕ_p are small enough, i.e., $\|\mathbf{u}_f^k - \mathbf{u}_f^{k-1}\|_{l^2} + \|p_f^k - p_f^{k-1}\|_{l^2} + \|\phi_p^k - \phi_p^{k-1}\|_{l^2} \leq \epsilon$ where $\epsilon = 10^{-5}$. Convergence analysis of this algorithm can be found in [30, 21, 15]. We refer readers to that elegant proof.

2.2 Robin-Robin DDM with BJ interface conditions

In the previous section, we investigated the Stokes-Darcy system with BJS interface condition. In this section, we focus on the same system but coupled with BJ interface condition. There are several differences between BJS and BJ interface conditions. First, the well-posedness of the whole Stokes-Darcy Structure with BJS interface condition is established and proved. This system is more deeply investigated into by scientists and researchers compared with the BJ system. However, the well posedness of BJ interface condition is recently demonstrated. It is shown that BJ system is well posed if a certain parameter is small enough [21, 17, 20, 39]. We introduce this parameter and formulation in the following discussion. Secondly, BJS interface conditions fail to fully account for the properties of the porous media flow. For example, the model of Karst aquifers is not representable by Stokes-Darcy Structure Interaction with BJS interface conditions, while BJ interface conditions are more physically relevant and provide better accuracy.

Along the interface Γ, let's define three interface conditions:

$$\mathbf{u}_f \cdot \mathbf{n}_f = -\mathbf{u}_p \cdot \mathbf{n}_p. \tag{2.29}$$

The second interface condition is the balance of normal stress across Γ

$$-\mathbf{n}_f \cdot (\mathbf{T}(\mathbf{u}_f, p_f) \cdot \mathbf{n}_f) = g(\phi_p - z). \tag{2.30}$$

Finally, the so called Beavers-Joseph (BJ) interface condition

$$-\tau_j \cdot (\mathbf{T}(\mathbf{u}_f, p_f) \cdot \mathbf{n}_f) = \frac{\alpha \nu \sqrt{\mathbf{d}}}{\sqrt{\text{trace}(\Pi)}} \tau_j \cdot (\mathbf{u}_f - \mathbf{u}_p), \tag{2.31}$$

where $\mathbf{n}_f$ denote the unit outward normal vector from Ω_f at Γ and $\mathbf{n}_p$ denote outward normal vector from Ω_p at Γ. τ_j $(j = 1, ..., d-1)$ represents unit tangential vectors on Γ following right hand rule. $\Pi = \frac{\mathbf{K}\nu}{g}$ is some constant matrix. α is exchange coefficient, when this quantity is sufficiently small and $\mathbf{K}$ is isotropic, the well posedness of this coupled Stokes-Darcy system can be shown.

2.2.1 Weak Formulation

We assume ϕ_p and $\mathbf{u}_f$ are 0 on the boundary $\partial\Omega$ and define the following functional spaces

$$H_f = \{\mathbf{v}_f \in (H^1(\Omega_f))^d | \mathbf{v}_f = 0 \text{ on } \partial\Omega_f \backslash \Gamma\}, \tag{2.32}$$

$$Q = L^2(\Omega_f), \tag{2.33}$$

$$H_p = \{\psi_p \in H^1(\Omega_p) | \psi_p = 0 \text{ on } \partial\Omega_p \backslash \Gamma\}. \tag{2.34}$$

The following bilinear forms are defined as

$$
\begin{aligned}
a_f(\mathbf{u}_f, \mathbf{v}_f) &= 2\nu(\mathbf{D}(\mathbf{u}_f), \mathbf{D}(\mathbf{v}_f)) \quad \text{on } \Omega_f, && (2.35)\\
a_p(\phi_p, \psi_p) &= (\mathbf{K}\nabla\phi_p, \nabla\psi_p) \qquad \text{on } \Omega_p, && (2.36)\\
b_f(\mathbf{v}_f, p_f) &= -(\nabla\cdot\mathbf{v}_f, p_f) \qquad \text{on } \Omega_f. && (2.37)
\end{aligned}
$$

From [30, 21, 15], the weak formulation of the coupled system becomes: finding $(\mathbf{u}_f, p_f)$ $\in H_f \times Q$, $\phi_p \in H_p$ such that

$$
\begin{aligned}
a_f(\mathbf{u}_f, \mathbf{v}_f) + b_f(\mathbf{v}_f, p_f) &+ a_p(\phi_p, \psi_p) + \langle g\phi_p, \mathbf{v}_f\cdot\mathbf{n}_f\rangle\\
-\langle \mathbf{u}_f\cdot\mathbf{n}_f, \psi_p\rangle &+ \frac{\alpha\nu\sqrt{\mathbf{d}}}{\sqrt{\text{trace}(\Pi)}}\langle \mathbf{P}_\tau(\mathbf{u}_f + \mathbf{K}\nabla\phi_p), \mathbf{P}_\tau\mathbf{v}_f\rangle\\
= (\mathbf{f}_f, \mathbf{v}_f) + (\mathbf{f}_p, \psi_p) &+ \langle gz, \mathbf{v}_f\cdot\mathbf{n}_f\rangle \quad \forall \mathbf{v}_f \in H_f, \psi_p \in H_p, && (2.38)\\
b_f(\mathbf{u}_f, q_f) &= 0 \quad \forall q_f \in Q, && (2.39)
\end{aligned}
$$

where $(\cdot,\cdot)$ denotes L^2 inner product, $\langle\cdot,\cdot\rangle$ denotes L^2 inner product along the interface Γ, again

$$
\mathbf{P}_\tau\mathbf{u}_\mathbf{f} = \sum_{j=1}^{d-1}(\mathbf{u}_f\cdot\tau_j)\tau_j. \tag{2.40}
$$

2.2.2 Robin-Robin DDM with BJ interface conditions

Next, we define the Robin-Robin domain decomposition method by imposing Robin boundary conditions for the coupled Stokes-Darcy system along the interface. Tildes are added on certain variables to distinguish them from previous notations.

First, let's consider the Robin boundary condition for the Stokes system

$$\mathbf{n}_f \cdot (\mathbf{T}(\tilde{\mathbf{u}}_f, \tilde{p}_f) \cdot \mathbf{n}_f) + \gamma_f \tilde{\mathbf{u}}_f \cdot \mathbf{n}_f = \eta_f \quad \text{on } \Gamma, \tag{2.41}$$

$$\mathbf{P}_\tau(\mathbf{T}(\tilde{\mathbf{u}}_f, \tilde{p}_f) \cdot \mathbf{n}_f) - \frac{\alpha \nu \sqrt{\mathbf{d}}}{\sqrt{\text{trace}(\Pi)}} \mathbf{P}_\tau \tilde{\mathbf{u}}_f = \boldsymbol{\eta}_{f\tau} \quad \text{on } \Gamma \tag{2.42}$$

where $\gamma_f > 0$ is a constant, η_f and $\boldsymbol{\eta}_{f\tau}$ are functions evaluated on Γ. With this Robin boundary condition defined on Γ, the weak formulation for the Stokes equations becomes: finding $(\tilde{\mathbf{u}}_f, \tilde{p}_f) \in H_f \times Q$, η_f, $\boldsymbol{\eta}_{f\tau} \in L^2(\Gamma)$ such that

$$\begin{aligned} a_f(\tilde{\mathbf{u}}_f, \mathbf{v}_f) + b_f(\mathbf{v}_f, \tilde{p}_f) &+ \gamma_f \langle \tilde{\mathbf{u}}_f \cdot \mathbf{n}_f, \mathbf{v}_f \cdot \mathbf{n}_f \rangle + \frac{\alpha \nu \sqrt{\mathbf{d}}}{\sqrt{\text{trace}(\Pi)}} \langle \mathbf{P}_\tau \tilde{\mathbf{u}}_f, \mathbf{P}_\tau \mathbf{v}_f \rangle \\ &= (\mathbf{f}, \mathbf{v}_f) + \langle \eta_f, \mathbf{v}_f \cdot \mathbf{n}_f \rangle - \langle \boldsymbol{\eta}_{f\tau}, \mathbf{P}_\tau \mathbf{v}_f \rangle \quad \forall \mathbf{v}_f \in H_f, \end{aligned} \tag{2.43}$$

$$b_f(\tilde{\mathbf{u}}_f, q_f) = 0 \quad \forall q_f \in Q. \tag{2.44}$$

Next consider the Robin boundary condition for Darcy's law

$$\gamma_p \mathbf{K} \nabla \tilde{\phi}_p \cdot \mathbf{n}_p + g \tilde{\phi}_p = \eta_p \quad \text{on } \Gamma, \tag{2.45}$$

where $\gamma_p > 0$ is a constant and η_p is a function defined similar to η_f unless on Ω_p. The weak formulation of Darcy's law becomes: finding $\tilde{\phi}_p \in H_p$, $\eta_p \in L^2(\Gamma)$ such that

$$\gamma_p a_p(\tilde{\phi}_p, \psi_p) + \langle g \tilde{\phi}_p, \psi_p \rangle = \langle \eta_p, \psi_p \rangle + \gamma_p (f_p, \psi_p) \quad \forall \psi_p \in H_p. \tag{2.46}$$

Again, we combine these weak formulations together in two one large equation system. If η_f, $\boldsymbol{\eta}_{f\tau}$ and η_p are given, there exists a unique solution $(\tilde{\mathbf{u}}_f, \tilde{p}_f) \in H_f \times Q$, $\tilde{\phi}_p \in H_p$ such

that

$$
\begin{aligned}
a_f(\tilde{\mathbf{u}}_f, \mathbf{v}_f) + b_f(\mathbf{v}_f, \tilde{p}_f) &+ \gamma_f \langle \tilde{\mathbf{u}}_f \cdot \mathbf{n}_f, \mathbf{v}_f \cdot \mathbf{n}_f \rangle \\
+\frac{\alpha \nu \sqrt{\mathbf{d}}}{\sqrt{\text{trace}(\Pi)}} \langle \mathbf{P}_\tau \tilde{\mathbf{u}}_f, \mathbf{P}_\tau \mathbf{v}_f \rangle &+ \gamma_p a_p(\tilde{\phi}_p, \psi_p) + \langle g\tilde{\phi}_p, \psi_p \rangle \\
= (\mathbf{f}, \mathbf{v}_f) &+ \langle \eta_f, \mathbf{v}_f \cdot \mathbf{n}_f \rangle - \langle \boldsymbol{\eta}_{f\tau}, \mathbf{P}_\tau \mathbf{v}_f \rangle \\
+\langle \eta_p, \psi_p \rangle &+ \gamma_p (f_p, \psi_p) \quad \forall \mathbf{v}_f \in H_f, \psi_p \in H_p, \qquad (2.47) \\
b_f(\tilde{\mathbf{u}}_f, q_f) &= 0 \quad \forall q_f \in Q. \qquad (2.48)
\end{aligned}
$$

Finally, to determine appropriate values of functions η_f, $\boldsymbol{\eta}_{f\tau}$ and η_p, we refer back to equations (2.38), (2.39), which are the weak formulations of the Stokes-Darcy system with BJ interface condition. Equations (2.38), (2.39) and (2.47), (2.48) are consistent, i.e., $\mathbf{u}_f = \tilde{\mathbf{u}}_f$, $p_f = \tilde{p}_f$ and $\phi_p = \tilde{\phi}_p$. By subtracting (2.38), (2.39) and (2.47), (2.48), we can get the following equation

$$
\begin{aligned}
&\langle \eta_p - \gamma_p \mathbf{u}_f \cdot \mathbf{n}_f - g\phi_p, \psi_p \rangle \qquad (2.49) \\
+ \quad &\langle \eta_f - \gamma_f \mathbf{u}_f \cdot \mathbf{n}_f + g\phi_p - gz, \mathbf{v}_f \cdot \mathbf{n}_f \rangle \\
+ \quad &\langle \eta_{f\tau} - \frac{\alpha \nu \sqrt{\mathbf{d}}}{\sqrt{\text{trace}(\Pi)}} \mathbf{P}_\tau(\mathbf{K} \nabla \phi_p), \mathbf{P}_\tau \mathbf{v}_f \rangle = 0 \quad \forall \mathbf{v}_f \in H_f, \psi_p \in H_p.
\end{aligned}
$$

As equation (2.50) is valid for arbitrary test functions ψ_p, $\mathbf{v}_f$, we first choose $\mathbf{v}_f$ such that $\mathbf{v}_f \cdot \mathbf{n}_f = 0$ and $\mathbf{P}_\tau \mathbf{v}_f = 0$, therefore we could have the following condition

$$
\langle \eta_p - \gamma_p \mathbf{u}_f \cdot \mathbf{n}_f - g\phi_p, \psi_p \rangle = 0. \qquad (2.50)
$$

Because ψ_p is arbitrary and the Stokes- Darcy system is well-posed and therefore unique,

we could have

$$\eta_p = \gamma_p \mathbf{u}_f \cdot \mathbf{n}_f + g\phi_p. \tag{2.51}$$

Similarly, by letting $\psi_p = 0$ and $\mathbf{P}_\tau \mathbf{v}_f = 0$, we have

$$\eta_f = \gamma_f \mathbf{u}_f \cdot \mathbf{n}_f - g\phi_p + gz. \tag{2.52}$$

By letting $\mathbf{v}_f \cdot \mathbf{n}_f = 0$ and $\mathbf{P}_\tau \mathbf{v}_f = 0$, we have

$$\boldsymbol{\eta}_{f\tau} = \frac{\alpha \nu \sqrt{\mathbf{d}}}{\sqrt{\text{trace}(\Pi)}} \mathbf{P}_\tau (\mathbf{K} \nabla \phi_p). \tag{2.53}$$

In summary, Stokes-Darcy system with BJ interface condition and Stokes-Darcy system with Robin-Robin boundary condition are compatible if and only if the following compatibility condition hold

$$\begin{aligned} \eta_p &= \gamma_p \mathbf{u}_f \cdot \mathbf{n}_f + g\phi_p, \\ \eta_f &= \gamma_f \mathbf{u}_f \cdot \mathbf{n}_f - g\phi_p + gz, \\ \boldsymbol{\eta}_{f\tau} &= \frac{\alpha \nu \sqrt{\mathbf{d}}}{\sqrt{\text{trace}(\Pi)}} \mathbf{P}_\tau (\mathbf{K} \nabla \phi_p). \end{aligned} \tag{2.54}$$

The necessity can be validated by the above argument. For sufficiency, sustituting equations 2.54 back into (2.38), (2.39), which obviously solve the coupled equation system. In light of the well-posedness of the system under the condition α is small enough and $\mathbf{K}$ is isotropic. As the solution is unique, the sufficient condition is proved. In other words, $\mathbf{u}_f = \tilde{\mathbf{u}}_f$, $p_f = \tilde{p}_f$ and $\phi_p = \tilde{\phi}_p$. We can solve the latter one, which is Robin-Robin Stokes-Darcy system instead.

In this way, we have the following algorithm of Robin-Robin domain decomposition method [30, 21, 15]:

Step 1: For $k = 1, 2, \ldots$, solve the Stokes system (2.43),(2.44) and the Darcy system (2.46) separately, i.e., finding $(\mathbf{u}_f^k, p_f^k) \in H_f \times Q$, $\phi_p^k \in H_p$ such that

$$\begin{aligned} a_f(\mathbf{u}_f^k, \mathbf{v}_f) &+ b_f(\mathbf{v}_f, p_f^k) + \gamma_f \langle \mathbf{u}_f^k \cdot \mathbf{n}_f, \mathbf{v}_f \cdot \mathbf{n}_f \rangle \\ &+ \frac{\alpha \nu \sqrt{\mathbf{d}}}{\sqrt{\text{trace}(\Pi)}} \langle \mathbf{P}_\tau \mathbf{u}_f^k, \mathbf{P}_\tau \mathbf{v}_f \rangle \\ &= (\mathbf{f}, \mathbf{v}_f) + \langle \eta_f^k, \mathbf{v}_f \cdot \mathbf{n}_f \rangle \qquad (2.55) \\ &- \langle \boldsymbol{\eta}_{f\tau}^k, \mathbf{P}_\tau \mathbf{v}_f \rangle \quad \forall \mathbf{v}_f \in H_f, \\ b_f(\mathbf{u}^{\mathbf{k}}{}_f, q_f) &= 0 \quad \forall q_f \in Q, \qquad (2.56) \\ \gamma_p a_p(\phi_p^k, \psi_p) + \langle g \phi_p^k, \psi_p \rangle &= \langle \eta_p^k, \psi_p \rangle + \gamma_p (f_p, \psi_p) \quad \forall \psi_p \in H_p. \qquad (2.57) \end{aligned}$$

Step 2: η_f, $\eta_{f\tau}$ and η_p are updated at each loop as

$$\begin{aligned} \eta_f^{k+1} &= \frac{\gamma_f}{\gamma_p} \eta_p^k + \left(-1 - \frac{\gamma_f}{\gamma_p} \right) g \phi_p^k + gz, \qquad (2.58) \\ \boldsymbol{\eta}_{f\tau}^{k+1} &= \frac{\alpha \nu \sqrt{\mathbf{d}}}{\sqrt{\text{trace}(\Pi)}} \mathbf{P}_\tau (\mathbf{K} \nabla \phi_p^k), \qquad (2.59) \\ \eta_p^{k+1} &= -\eta_f^k + (\gamma_f + \gamma_p) \mathbf{u}_f^k \cdot \mathbf{n}_f + gz. \qquad (2.60) \end{aligned}$$

Initial values of η_f, $\boldsymbol{\eta}_{f\tau}$ and η_p are chosen arbitrarily. Conditions (2.58), (2.59), (2.60) are necessary for the convergence of this algorithm. The algorithm stops when the changes in $\mathbf{u}_f$, p_f and ϕ_p are small enough, i.e., $\|\mathbf{u}_f^k - \mathbf{u}_f^{k-1}\|_{l^2} + \|p_f^k - p_f^{k-1}\|_{l^2} + \|\phi_p^k - \phi_p^{k-1}\|_{l^2} \leq \epsilon$ where $\epsilon = 10^{-5}$.

2.3 Local Modified Cartesian Meshes

In this section, we explain how to get a locally modified Cartesian mesh from a uniform Cartesian mesh. The idea of this method is to perturb the triangulations while keeping the number of nodal points unchanged. The procedure is easy to follow and is shown below:

Step 1: Generate a Cartesian grid. For simplicity, in this paper, we consider a rectangular grid and take the step size the same in both x and y direction, Figure 2.1 shows mesh generated by unstructured method.

Step 2: Locate the intersection of the interface and the grid line. Figure 2.2 shows the grid lines and the location of the interface. If the intersection lies between $[x_i - h/2, x_i + h/2] \times [y_i - h/2, y_i + h/2]$, we call the point $[x_i, y_i]$ an irregular point. Otherwise, we call it a regular point.

Step 3: For each irregular point, replace it with an intersection point as a new nodal point. If there is more than one intersection point, the one with smallest distance to the irregular point will be taken. In Figure 2.3, the grid point P is an irregular point because the intersection point is within the small dashed rectangle. P1 and P2 are the intersection points. As the the distance $d(P, P1) < d(P, P2)$, we take P1 as a new nodal point as demonstrated in Figure 2.4.

Step 4: Use the modified nodal points to build triangulations and form a body fitted mesh.

It has been proven in [8] that if the interface $\Gamma \in \mathscr{C}^2$, the accuracy of the approximation of the interface Γ is $O(h^2)$. Figure 2.6 is an example of the locally modified mesh in which the interface is a circle. We can see that only the points around the circular interface are altered and the total number of nodal points remain unchanged.

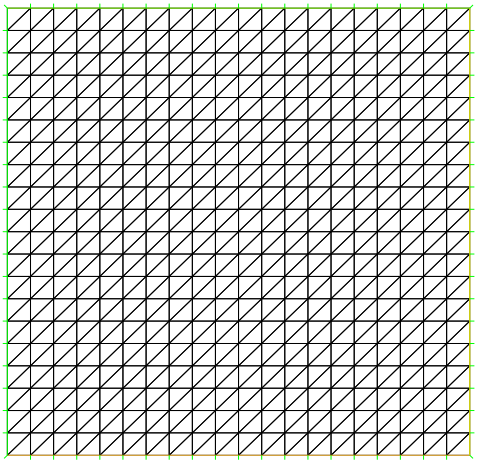

Figure 2.1: An example of Cartesian grid mesh.

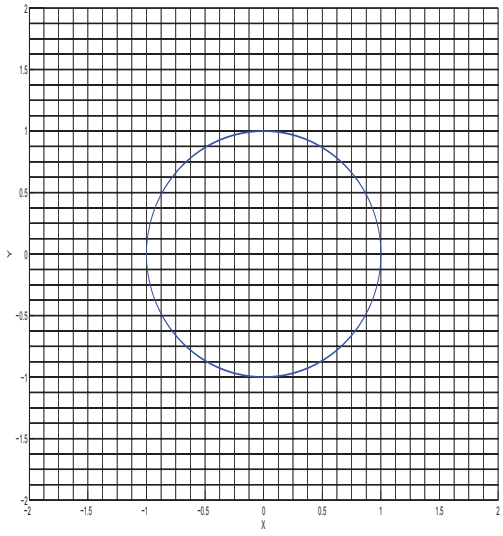

Figure 2.2: Sketch of the grid lines and the interface without mesh modifications.

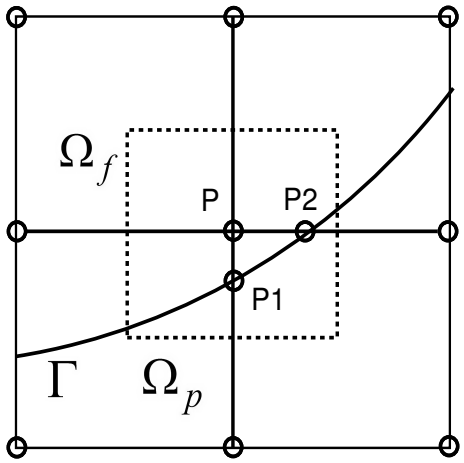

Figure 2.3: An example of an irregular point and the interface. P1 and P2 are the two points of the intersection between interface Γ and grid lines within the small dashed square $[x_i - h/2, x_i + h/2] \times [y_i - h/2, y_i + h/2]$ of irregular point P. The area on the left of Γ is Ω_f, on the right is Ω_p.

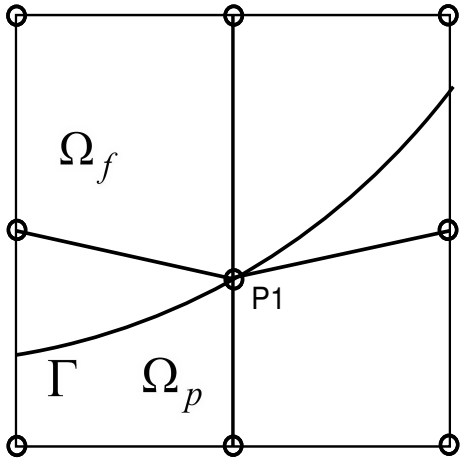

Figure 2.4: An example of a modified point. Point P is replaced by point P1 and the total number of nodal points remains unchanged.

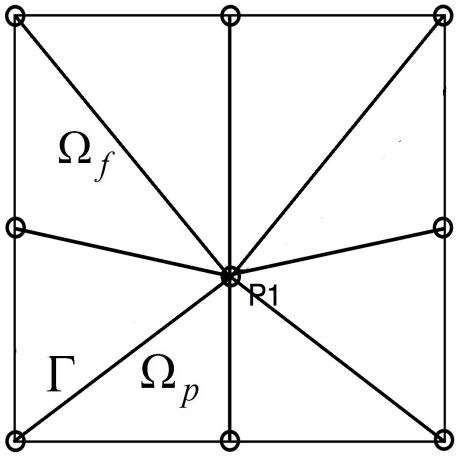

Figure 2.5: A triangulation based on the modified grid points.

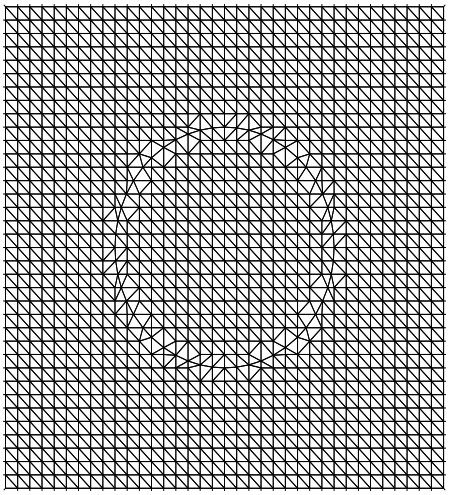

Figure 2.6: A locally modified mesh example where step number n=32 (32 points on each side of the square)in both x and y direction. The triangulations are built using the modified nodal points.

2.4 Numerical Examples for BJS Interface Conditions

In this section we present two numerical examples of the coupled nondimensional Stokes-Darcy system with a circular interface. Consider a case in $\mathbb{R}^2$. Let Ω_f be a unit circle centered at $(0,0)$ with radius 1. Ω_p is the square of $[-2,2]\times[-2,2]$ outside the unit circle. See Figure 2.7 as an illustration. The unstructured mesh is shown in Figure 2.8 while the locally modified mesh is constructed and is shown is Figure 2.6. For simplicity, choose $\nu = 1$, $g = 1$, $\mathbf{K} = \mathbf{I}$, $\alpha = 1$. An analytic solution of (2.38), (2.39) is given by

$$u_1 = y(x^2+y^2-3), \quad u_2 = -x(x^2+y^2-3), \quad p_f = x^2+y^2, \tag{2.61}$$
$$f_1 = -8y+2x, \quad f_2 = 8x+2y, \quad \phi_p = 1.$$

The boundary conditions on $\partial\Omega$ are determined accordingly. These analytic solutions satisfy the Stokes-Darcy system with circular interface as well as the BJS interface condition. For the finite element approximation, the Taylor-Hood element pair is used for the Stokes equations which is quadratic in velocity and linear in pressure. A linear finite element space is used for Darcy's law. The dimension of finite element space of the coupled Stokes-Darcy system is consistent on the interface.

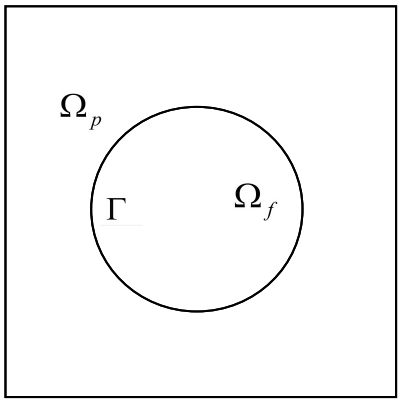

Figure 2.7: A computational example with circular interface Γ.

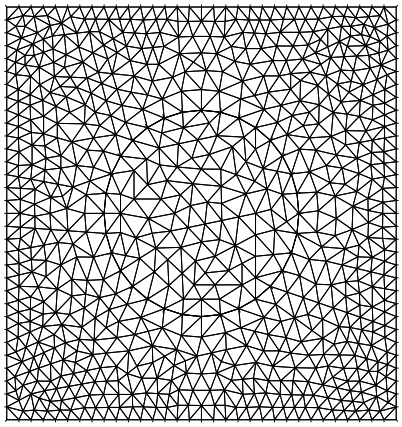

Figure 2.8: An unstructured mesh example where step number n=32 in both x and y direction.

As discussed in [30, 21, 15], we choose $\gamma_f = 3\gamma_p$ for convergence of the algorithm. In Table 2.1, the H^1 norm error of velocity $\mathbf{u}_f$, and the L^2 norm error of $\mathbf{u}_f$, p_f and ϕ_p are reported. Table 2.3 shows the error report based on locally modified mesh method. We compare the two methods (Table 2.15) for a locally modified mesh of 2048 elements and

an unstructured mesh of 2100 elements (260 Stokes, 1840 Darcy). The two methods have comparable error. Therefore the method of locally modified mesh is not only free of mesh generation, but also provides comparable accuracy. Table 2.16 compares convergence order as the slope of the log-log plots of error against grid fineness n. As usual, the H^1 norm error of $\mathbf{u}_f$ is approximately one order less than the L^2 norm error of $\mathbf{u}_f$. Figure 2.9 shows the velocity computed using the locally modified mesh for the example (3.15).

We now provide a more realistic example. In Figure 2.10, a simulation of the Stokes-Darcy interaction is shown by assuming the fluid velocity on the boundary is $(0,-1)$. The parameter values ν, g, $\mathbf{K}$ and α are set the same as in the previous example. The overall flow is downwards with faster flow in the Stokes region due to the coupling at the interface, corresponding to flow in a void in a porous medium such as soil. Moreover, a grid refinement analysis is conducted to test the convergence order of this method. Different step number n are compared with a fine grid $n = 160$. Because we are not comparing our results with a much finer grid, the covergence order is not 2 for a first order method, or 4 for a second order method. In this case

$$\frac{\|\mathbf{u}_f^{40} - \mathbf{u}_f^{160}\|_{l_2}}{\|\mathbf{u}_f^{80} - \mathbf{u}_f^{160}\|_{l_2}} \approx \frac{4^q - 1}{2^q - 1}. \tag{2.62}$$

For $q = 1$, the ratio becomes 3, while for $q = 2$, the ratio becomes 5 where q is the order of convergence. In Table 2.7, 2.8, 2.9 and 2.10, we can see the two methods roughly have the same order of ratio. As a result, the unstructured mesh method and locally modified mesh method provide comparable accuracy. See[55] for more details on mesh refinement analysis.

Table 2.1: An error report of unstructured mesh method with various step numbers.

Step number n	L^2 error of $\mathbf{u}_f$	H^1 error of $\mathbf{u}_f$	L^2 error of p_f	L^2 error of ϕ_p	Iterations
16	7.83e-2	2.02e-1	5.34e-2	1.61e-2	30
32	2.02e-2	8.29e-2	2.09e-2	8.02e-3	30
64	5.01e-3	5.02e-2	4.11e-3	3.84e-3	31
128	1.28e-3	3.53e-2	2.41e-3	2.02e-3	31

Table 2.2: An error report of unstructured mesh method with another set of step numbers.

Step number n	L^2 error of $\mathbf{u}_f$	H^1 error of $\mathbf{u}_f$	L^2 error of p_f	L^2 error of ϕ_p	Iterations
20	5.11e-2	1.45e-1	4.31e-2	1.26e-2	30
40	1.29e-2	6.80e-2	1.31e-2	6.20e-3	30
80	3.25e-3	4.34e-2	3.08e-3	3.11e-3	31
160	8.2e-4	2.20e-2	1.21e-3	1.56e-3	31

Table 2.3: An error report of locally modified mesh method with various step numbers.

Step number n	L^2 error of $\mathbf{u}_f$	H^1 error of $\mathbf{u}_f$	L^2 error of p_f	L^2 error of ϕ_p	Iterations
16	3.74e-2	1.14e-1	4.21e-2	1.07e-2	29
32	1.18e-2	6.36e-2	1.20e-2	6.36e-3	29
64	2.50e-3	4.11e-2	3.40e-3	2.94e-3	30
128	6.70e-4	2.90e-2	2.01e-3	1.71e-3	30

Table 2.4: An error report of locally modified mesh method with another set of step numbers.

Step number n	L^2 error of $\mathbf{u}_f$	H^1 error of $\mathbf{u}_f$	L^2 error of p_f	L^2 error of ϕ_p	Iterations
20	2.73e-2	9.71e-2	2.71e-2	1.06e-2	29
40	6.90e-3	5.40e-2	7.61e-3	5.26e-3	29
80	1.75e-3	3.74e-2	2.91e-3	2.57e-3	30
160	4.41e-4	1.90e-2	7.92e-4	1.29e-3	30

Table 2.5: A comparison of the two methods based on a similar number of triangulations.

Method	Elements	L^2 error of $\mathbf{u}_f$	H^1 error of $\mathbf{u}_f$	L^2 error of p_f	L^2 error of ϕ_p
unstructured mesh	2100	1.43e-2	7.11e-2	5.74e-3	6.70e-3
locally modified mesh	2048	1.18e-2	6.36e-2	1.20e-3	6.36e-3

Table 2.6: A comparison of the convergence order of unstructured mesh and locally modified mesh.

		Unstructured mesh		Locally modified mesh	
Quantity	Norm	Slope	R^2	Slope	R^2
$\mathbf{u}_f$	L^2	1.98	0.99	1.97	0.99
$\mathbf{u}_f$	H^1	0.83	0.96	0.67	0.98
p_f	L^2	1.67	0.97	1.44	0.96
ϕ_p	L^2	1.01	0.99	0.94	0.99

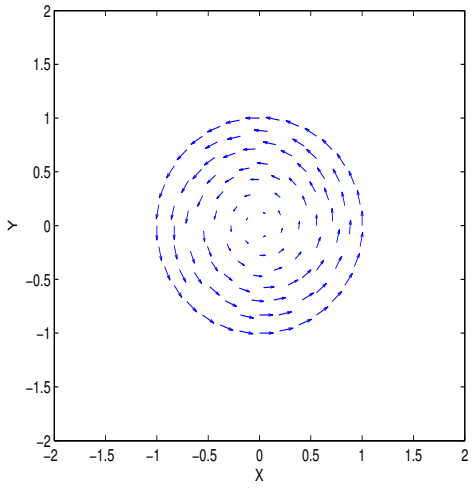

Figure 2.9: A plot of the fluid velocity in the coupled Stokes-Darcy system for the example (3.15). As Φ_p=1, the fluid velocity in porous media region Ω_p, in this case, outside the unit circle, is 0.

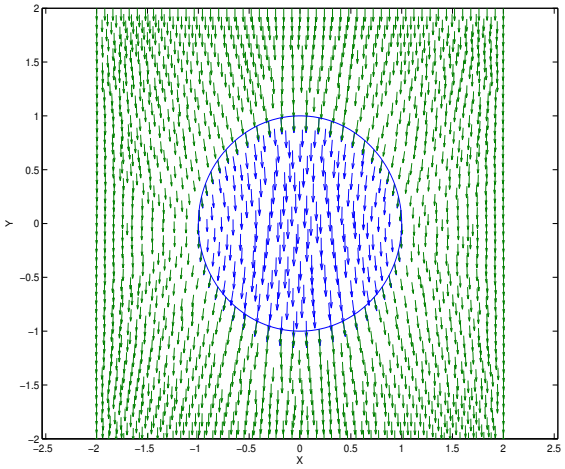

Figure 2.10: A simulation of the Stokes-Darcy interaction with parameters $\nu = 1$, $g = 1$, $\mathbf{K} = \mathbf{I}$ and $\alpha = 1$. The fluid of Darcy's law moves downwards and interacts with the fluid of Stokes equations.

Table 2.7: An error report for a grid refinement analysis of unstructured mesh method in $\mathbf{u}_f$.

Step number n	$\|\mathbf{u}_f^N - \mathbf{u}_f^{160}\|_{l_2}$	r_1	$\|\mathbf{u}_f^N - \mathbf{u}_f^{160}\|_{h_1}$	r_2	Iterations
20	1.64e-2		1.31e-2		28
40	2.41e-3	6.31	4.11e-2	2.94	28
80	4.79e-4	5.03	1.59e-2	2.58	26

Table 2.8: An error report for a grid refinement analysis of unstructured mesh method in p_f and ϕ_p.

Step number n	$\|p_f^N - p_f^{160}\|_{l_2}$	r_3	$\|\phi_p^N - \phi_p^{160}\|_{l_2}$	r_4	Iterations
20	1.52e-2		1.21e-1		28
40	2.78e-2	5.94	4.34e-2	2.79	28
80	5.21e-3	5.32	1.73e-2	2.51	26

Table 2.9: An error report for a grid refinement analysis of locally modified mesh method in $\mathbf{u}_f$.

Step number n	$\|\mathbf{u}_f^N - \mathbf{u}_f^{160}\|_{l_2}$	r_5	$\|\mathbf{u}_f^N - \mathbf{u}_f^{160}\|_{h_1}$	r_6	Iterations
20	4.33e-2		1.87e-1		28
40	6.62e-3	6.54	6.19e-2	3.02	28
80	1.24e-3	5.34	2.23e-2	2.77	26

Table 2.10: An error report for a grid refinement analysis of locally modified mesh method in p_f and ϕ_p.

Step number n	$\|p_f^N - p_f^{160}\|_{l_2}$	r_7	$\|\phi_p^N - \phi_p^{160}\|_{l_2}$	r_8	Iterations
20	3.13e-2		1.12e-1		28
40	5.42e-3	5.77	3.61e-2	3.10	28
80	1.01e-3	5.40	1.29e-2	2.81	26

2.5 Numerical Examples for BJ Interface Conditions

In this section we disciss some numerical experiments of the coupled nondimensional Stokes-Darcy system with BJ interface conditions. We consider a case in $\mathbb{R}^2$. Let Ω_f be a unit circle centered at $(0,0)$ with radius 1. Ω_p is an ellipse of $[-3,3]\times[-2,2]$ outside the unit circle. See Figure 2.11 as an example. Computations using unstructured mesh and locally modified mesh are compared and discussed. For simplicity, choose $\nu = 1$, $g = 1$, $z = 1$, $\mathbf{K} = \mathbf{I}$, $\alpha = 1$, $d = 2$, trace$(\Pi) = 2$. An analytic solution the system is given by

$$u_1 = y(x^2+y^2-3), \quad u_2 = -x(x^2+y^2-3), \quad p_f = x^2+y^2+1, \tag{2.63}$$
$$f_1 = -8y+2x, \quad f_2 = 8x+2y, \quad \phi_p = 2.$$

The boundary conditions on $\partial\Omega_p$ are determined accordingly. The system is defined on an ellipse interface. For the finite element approximation, the Taylor-Hood element pair is used for the Stokes equations, which is quadratic in velocity and linear in pressure. A linear finite element space is prescribed for the Darcy's law. The dimension of finite element space of the coupled Stokes-Darcy system is consistent on the interface.

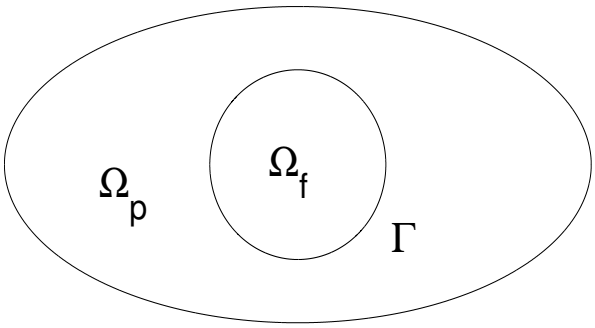

Figure 2.11: A computational example with circular interface Γ.

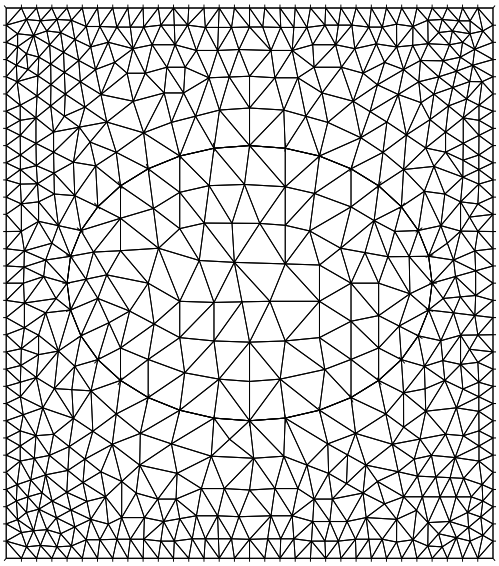

Figure 2.12: An unstructured mesh example where step number n=32 on both interior and exterior boundary.

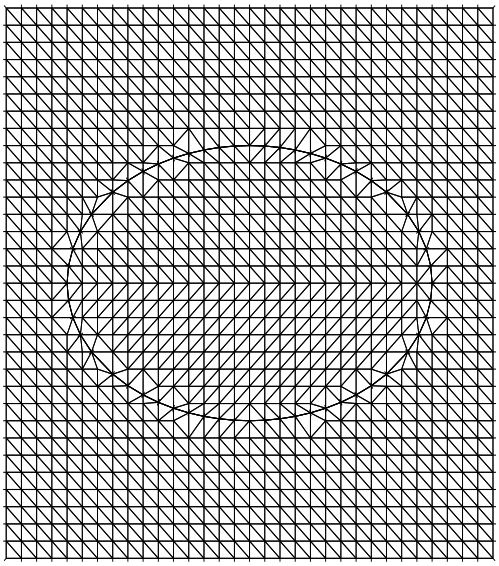

Figure 2.13: A locally modified mesh example where step number n=32 on both interior and exterior boundary.

We choose $\gamma_p = 3\gamma_f$ for convergence of the algorithm. Both unstructured mesh and locally modified mesh are constructed, see Figure 2.12, 2.13 as examples. In those two figures, we take 32 steps in both x and y direction. For 2.13, we can easily see only the points near the ellipse interface is changed while other points stay the same. This method reduces the time cost of the mesh generation process as discussed in last chapter. The CPU time of unstructured mesh generation is 0.14s compared with 0.05s of locally modified mesh.

In Table 2.11, the H^1 norm error of velocity $\mathbf{u}_f$, and the L^2 norm error of $\mathbf{u}_f$, p_f and ϕ_p are reported. Table 2.13 shows the error report based on locally modified mesh method. We compare the two methods (Table 2.15) for a locally modified mesh of 2048 elements and an unstructured mesh of 2100 elements (260 Stokes, 1840 Darcy). The two methods again have comparable error. Table 2.16 compares convergence order as the slope of the log-log

plots of error against grid fineness n. As usual, the H^1 norm error of $\mathbf{u}_f$ is approximately one order lower than the L^2 norm error of $\mathbf{u}_f$.

Moreover, we consider another test problem. For the same two meshes, we assume the fluid velocity on the boundary for the Darcy's law to be (x^2, y^2). The parameter values ν, g, $\mathbf{K}$ and α are set the same as in the previous example. Again, we test this problem with grid refinement analysis discussed in the previous section. In Table 2.17, 2.18, 2.19 and 2.20, we can see the two methods roughly have the same order of ratio. As a result, the unstructured mesh method and locally modified mesh method provide comparable accuracy.

Table 2.11: An error report of unstructured mesh method with various step numbers.

Step number n	L^2 error of $\mathbf{u}_f$	H^1 error of $\mathbf{u}_f$	L^2 error of p_f	L^2 error of ϕ_p	Iterations
16	7.41e-2	2.35e-1	5.48e-2	1.48e-2	30
32	1.82e-2	8.01e-2	1.89e-2	7.5e-3	30
64	4.80e-3	4.84e-2	4.02e-3	3.75e-3	30
128	1.21e-3	2.53e-2	2.21e-3	1.90e-3	30

Table 2.12: An error report of unstructured mesh method with another set of step numbers.

Step number n	L^2 error of $\mathbf{u}_f$	H^1 error of $\mathbf{u}_f$	L^2 error of p_f	L^2 error of ϕ_p	Iterations
20	4.99e-2	1.38e-1	4.18e-2	1.18e-2	30
40	1.24e-2	6.87e-2	1.27e-2	6.01e-3	30
80	3.11e-3	3.86e-2	3.12e-3	3.08e-3	30
160	7.90e-4	1.99e-2	1.03e-3	1.51e-3	30

Table 2.13: An error report of locally modified mesh method with various step numbers.

Step number n	L^2 error of $\mathbf{u}_f$	H^1 error of $\mathbf{u}_f$	L^2 error of p_f	L^2 error of ϕ_p	Iterations
16	3.52e-2	1.08e-1	4.11e-2	1.12e-2	30
32	1.08e-2	6.12e-2	1.10e-2	6.16e-3	30
64	2.49e-3	3.96e-2	3.21e-3	2.65e-3	29
128	6.40e-4	2.70e-2	1.89e-3	1.61e-3	29

Table 2.14: An error report of locally modified mesh method with another set of step numbers.

Step number n	L^2 error of $\mathbf{u}_f$	H^1 error of $\mathbf{u}_f$	L^2 error of p_f	L^2 error of ϕ_p	Iterations
20	2.53e-2	9.42e-2	2.68e-2	1.08e-2	30
40	6.81e-3	5.30e-2	7.49e-3	5.10e-3	30
80	1.70e-3	3.54e-2	2.71e-3	2.60e-3	29
160	4.30e-4	1.78e-2	9.31e-4	1.30e-3	29

Table 2.15: A comparison of the two methods based on a similar number of triangulations.

Method	Elements	L^2 error of $\mathbf{u}_f$	H^1 error of $\mathbf{u}_f$	L^2 error of p_f	L^2 error of ϕ_p
unstructured mesh	2100	1.38e-2	7.01e-2	5.50e-3	6.56e-3
locally modified mesh	2048	1.01e-2	6.12e-2	1.01e-3	6.13e-3

Table 2.16: A comparison of the convergence order of unstructured mesh and locally modified mesh.

		Unstructured mesh		Locally modified mesh	
Quantity	Norm	Slope	R^2	Slope	R^2
$\mathbf{u}_f$	L^2	1.98	0.98	1.98	0.99
$\mathbf{u}_f$	H^1	0.83	0.96	0.78	0.98
p_f	L^2	1.70	0.97	1.52	0.96
ϕ_p	L^2	1.01	0.99	0.98	0.99

Table 2.17: An error report for a grid refinement analysis of unstructured mesh method in $\mathbf{u}_f$.

Step number n	$\|\mathbf{u}_f^N - \mathbf{u}_f^{160}\|_{l_2}$	r_1	$\|\mathbf{u}_f^N - \mathbf{u}_f^{160}\|_{h_1}$	r_2	Iterations
20	2.89e-2		1.78e-2		26
40	4.91e-3	5.89	6.18e-2	2.88	26
80	9.56-4	5.13	2.39e-2	2.59	24

Table 2.18: An error report for a grid refinement analysis of unstructured mesh method in p_f and ϕ_p.

Step number n	$\|p_f^N - p_f^{160}\|_{l_2}$	r_3	$\|\phi_p^N - \phi_p^{160}\|_{l_2}$	r_4	Iterations
20	1.72e-2		1.56e-1		26
40	2.92e-3	5.90	4.86e-2	3.21	26
80	5.94e-4	4.91	1.75e-2	2.77	24

Table 2.19: An error report for a grid refinement analysis of locally modified mesh method in $\mathbf{u}_f$.

Step number n	$\|\mathbf{u}_f^N - \mathbf{u}_f^{160}\|_{l_2}$	r_5	$\|\mathbf{u}_f^N - \mathbf{u}_f^{160}\|_{h_1}$	r_6	Iterations
20	7.88e-2		3.42e-1		26
40	1.29e-2	6.11	1.28e-1	2.67	26
80	2.48e-3	5.21	5.21e-2	2.46	24

Table 2.20: An error report for a grid refinement analysis of locally modified mesh method in p_f and ϕ_p.

Step number n	$\|p_f^N - p_f^{160}\|_{l_2}$	r_7	$\|\phi_p^N - \phi_p^{160}\|_{l_2}$	r_8	Iterations
20	3.21e-2		1.24e-1		26
40	6.21e-3	5.17	4.86e-2	2.55	26
80	1.30e-3	4.77	2.10e-2	2.32	24

2.6 Conclusions

We discussed the Stokes-Darcy system. A set of analytic solutions is constructed for the coupled system with a circular interface. The methods of locally modified mesh and unstructured mesh are compared and the Robin-Robin domain decomposition with locally modified mesh provides comparable accuracy and convergence order to that with an unstructured mesh. For the Stokes-Darcy system with complex domain structures, the Robin-Robin domain decomposition method based on a locally modified mesh might be more efficient then a potentially costly unstructured mesh.

Chapter 3

An Accurate Gradient Computation Method

.

3.1 Background

As we can see in the previous chapters, the error estimate of a variable's gradient is usually one order lower than the variable itself. In some scenarios, an accurately computed gradient is more desirable. In [12, 13, 14, 86], the finite element method is applied to Stokes equations where the equations are transformed to a pseudostress-velocity formulation. In this chapter, our objective is to introduce a new numerical method based on an augmented varable approach which provides better gradient accuracy near the boundary or the interface. The method is tested on a Poisson equation with a circular domain. In our result, an improved accuracy of gradient is obtained near the boundary/interface and an enlarged rectangular system is constructed.

3.2 Formulation

Define a Poisson equation on a circular domain. For simplification, let's consider a case in $\mathbb{R}^2$. Let Ω_1 be a unit circle centered at $(0,0)$ with radius 1. Let Γ be an interface inside the unit circle. Between the interface and the boundary, we have a small tube, denote this region as Ω_2. See Figure 3.1 as an illustration.

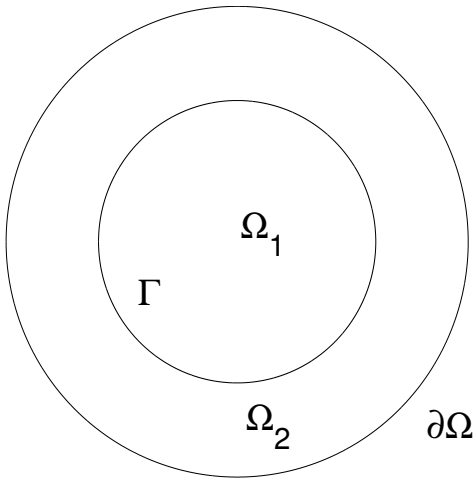

Figure 3.1: Sketch of domains Ω_1, Ω_2, the interface Γ, as well as boundary $\partial\Omega$.

On the whole domain Ω_1, a Poisson equation is defined with jump conditions in the coefficient β

$$-\nabla \cdot (\beta \nabla u) = f. \tag{3.1}$$

On the tube shaped domain Ω_2, a Poisson equation with augmented variables $\mathbf{v}$, which are

the gradient of u are defined

$$-\beta^+ \nabla u = \mathbf{v}, \tag{3.2}$$

$$\nabla \cdot \mathbf{v} = f. \tag{3.3}$$

$$\beta(\mathbf{x}) = \begin{cases} \beta^- & \text{if } \mathbf{x} \in \Omega_1, \\ \beta^+ & \text{if } \mathbf{x} \in \Omega_2, \end{cases} \tag{3.4}$$

where β^- and β^+ are some constants.

Next we derive the weak form. Assume w and u are 0 on the boundary $\partial\Omega$ and define the following functional spaces

$$H_1 = \{w \in (H^1(\Omega_1))^d | w = 0 \text{ on } \partial\Omega\}, \tag{3.5}$$

$$Q = L^2(\Omega_2), \tag{3.6}$$

$$H_2 = \{\mathbf{k} \in (H^1(\Omega_2))^d | \mathbf{k} = \mathbf{0} \text{ on } \partial\Omega\}. \tag{3.7}$$

To obtain the weak form, multiply test function w on both sides of the equaiton (3.1), integrate over the whole domain Ω_1 and integrate by part, we get

$$(\beta \nabla u, \nabla w) = (f, w) \quad \text{on } \Omega_1. \tag{3.8}$$

For the first equation (3.2) in the augmented system, multiply test function $\mathbf{k}$ on both sides, integrate over the domain Ω_2, we have

$$-(\beta^+ \nabla u, \mathbf{k}) = (\mathbf{v}, \mathbf{k}) \quad \text{on } \Omega_2. \tag{3.9}$$

For the second equation, multiply test function $q \in Q$ on both sides, integrate over the domain Ω_2, we have

$$(\nabla \cdot \mathbf{v}, q) = (f, q) \quad \text{on } \Omega_2. \tag{3.10}$$

In summary, we defined the following weak forms

$$\begin{aligned} (\beta \nabla u, \nabla w) &= (f, w) \qquad \text{on } \Omega_1, && (3.11)\\ -(\beta^+ \nabla u, \mathbf{k}) &= (\mathbf{v}, \mathbf{k}) \quad \text{on } \Omega_2, && (3.12)\\ (\nabla \cdot \mathbf{v}, q) &= (f, q) \qquad \text{on } \Omega_2. && (3.13) \end{aligned}$$

Therefore, the Poisson system is augmented on the outer domain Ω_2 along with the original system on the whole domain Ω_1.

3.3 Numerical Examples

In this section, we present some numerical examples of this augmented Poisson system. Consider a case in R^2. Let Ω_1 be a unit circle centered at (0, 0) with radius 1. The interface Γ is set to be $x^2 + y^2 = 0.9$. Ω_2 is a tube shaped region of the unit circle. Two finite element spaces are built up. The first one is based on the whole circular domain Ω_1, while the second one is built on the domain Ω_2. Unstructured meshes are generated for this example. See figure 3.2 as an illustration.

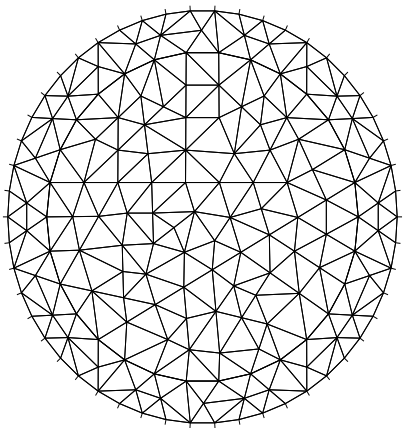

Figure 3.2: An unstructured mesh example where 50 steps are taken for the boundary $\partial\Omega$, 30 steps are taken for the interface Γ.

Consider a set of analytic solution

$$\begin{aligned} \beta^+ = 1, \quad \beta^- &= 100, \quad u = \sin(x)\cos(y), \\ \mathbf{v} = (v1, v2), \quad v1 &= -\cos(x)\cos(y), \quad v2 = \sin(x)\sin(y). \end{aligned} \tag{3.14}$$

The boundary conditions on $\partial\Omega$ are determined accordingly. For the finite element approximation, we used piecewise linear for both u and $\mathbf{v}$. The nodal points are consistent for the two finite element spaces. Routinely, our approach to a Poisson equation is to simply solve the equation (3.11). The new augmented method enlarged the system by (3.12) and (3.13). In terms of the stiffness matrix, an additional n_1 number of rows are added to the stiffness matrix where n_1 is the number of element in the domain Ω_2. An additional n_2 number of columns are added to the stiffness matrix where n_2 is the number of extra unknowns $v1$ and v_2. As a result, the stiffness matrix becomes a rectangular matrix instead of a square matrix. If we only consider the elements in domain Ω_2, the dimension of the

stiffness matrix is a $4n_1 \times 3n_1$. We used singular value decomposition (SVD) to solve this large rectangular system. In Table 3.1, the L^2 norm error of u, $\mathbf{v}$ and the H^1 norm error of u are reported. The step number m_1 is the number of steps we take along the boundary $\partial\Omega$. The step number m_2 is the number of steps we take along the interface Γ. To make it consistence, the ratio of $\frac{m_1}{m_2}$ is fixed to 2.

Table 3.1: An error report of augmented system with various step numbers.

Step number m_1	L^2 error of u	H^1 error of u	L^2 error of $\mathbf{v}$
8	9.96e-3	5.67e-1	5.67e-1
16	2.48e-3	1.75e-1	1.75e-1
32	7.77e-4	4.14e-2	4.14e-2
64	1.81e-4	1.04e-2	1.04e-2
128	4.71e-5	5.95e-3	5.95e-3
256	1.15e-5	1.54e-3	1.54e-3
512	2.92e-6	3.80e-4	3.80e-4

In Table 3.2, a comparison of the convergence order of routinely approach and augmented approach is presented. We can see the new approach provides better accuracy for the gradient computation.

Table 3.2: A comparison of the convergence order.

Quantity	Norm	Slope of original approach	Slope of new method
u	L^2	1.98	1.94
u	H^1	1.03	1.72
v	L^2	1.03	1.72

A comparison of the convergence order for various location of the interface is shown in Table 3.3. The first column means the location of the interface, i.e., $x^2 + y^2$ equals to the cell value. We can see the location of the interface has low impact on solution accuracy. Moreover, for the last row, where $x^2 + y^2 = 0$. We defined the augmented variables in the whole domain. Originally, we can only have first order accuracy in $\mathbf{v}$. In this case, the accuracy of gradient computation is improved by about 70 percent.

Table 3.3: A comparison of the convergence order for various location of the interface.

Interface	Slope of new method for L^2 norm of u	Slope of new method for H^1 norm of u
0.9	1.94	1.72
0.99	1.94	1.70
0	1.93	1.70

Next, consider another set of test problem

$$\begin{aligned} \beta^+ = 1, \quad \beta^- &= 10, \quad u = x^2 y^2, \\ \mathbf{v} = (v1, v2), \quad v1 &= -2xy^2, \quad v2 = -2x^2 y. \end{aligned} \tag{3.15}$$

We perform the similar discussion. In Table 3.4, we can see the error report.

Table 3.4: An error report of augmented system with various step numbers.

Step number m_1	L^2 error of u	H^1 error of u	L^2 error of $\mathbf{v}$
8	7.48e-3	4.21e-1	4.21e-1
16	1.91e-3	1.10e-1	1.10e-1
32	4.71e-4	2.81e-2	2.81e-2
64	1.21e-4	1.01e-2	1.01e-2
128	3.21e-5	4.74e-3	4.74e-3
256	7.76e-6	1.54e-3	1.54e-3
512	1.98e-6	4.77e-4	4.77e-4

In Table 3.5, a comparison of the convergence order of routinely approach and augmented approach is presented. We can see the new approach provides better accuracy for the gradient computation.

Table 3.5: A comparison of the convergence order.

Quantity	Norm	Slope of original approach	Slope of new method
u	L^2	1.96	1.95
u	H^1	1.01	1.74
v	L^2	1.01	1.74

A comparison of the convergence order for various location of the interface is shown in

Table 3.6.

Table 3.6: A comparison of the convergence order for various location of the interface.

Interface	Slope of new method for L^2 norm of u	Slope of new method for H^1 norm of u
0.9	1.94	1.74
0.99	1.94	1.71
0	1.93	1.71

3.4 Conclusions

In this chapter we introduced an augmented variable approach for accurate gradient computation near the boundary or the interface. Augmented variables, i.e., the gradient, is introduced on a small tube near the interface. This method is tested on a Poisson equation with a circular domain and a small tube. Our result showed an increased level of accuracy in gradient for nearly 70 percent. One tradeoff is that the stiffness matrix is transformed to an enlarged rectangular matrix with additional rows and columns. As a result, the computational cost is increased. Moreover, the location of the interface has small impact on the accuracy of gradient computation.

Chapter 4

Conclusions and Future Directions

.

In this dissertation, we focused on numerical methods and algorithms that apply to interface problems. Robin-Robin domain decomposition method was used to solve the coupled Stokes-Darcy system, while different interface conditions were investigated, such as BJ and BJS interface conditions. Additionally, numerical algorithms were analyzed and tested. To overcome the difficulties in mesh generation process, our method is coupled with the locally modified mesh method, which provides a solution to finite element discretization. Moreover, our method presents comparable accuracy and better efficiency in terms of mesh generation cost. Thus for large interface system such as Stokes-Darcy coupling, the problem can be solved with less requirements on computational memories and power. Furthermore, we introduced a new numerical method to accurately compute the gradient near the interface.

We summarize our contributions as below:

The first aspect is the accuracy. In our studies, finite element method was applied extensively to numerically solve a well-defined interface problem. For the coupled system

of Stokes-Darcy, Robin-Robin domain decomposition method with locally modified mesh method was constructed with second order accuracy, which meets researchers' expectation. This system was decoupled into each subdomain and solved separately. Morevoer, We showed this method provides a way where Stokes and Darcy systems can communicate and exchange information along the interface according to the algorithm. The locally modified mesh method was shown to provide comparable accuracy with unstructured mesh method. Finally, the accurate gradient computation method also illustrated an improved level of accuracy by introducing augmented variables.

The second focus is on the efficiency. To reduce the time cost of the mesh generation process, locally modified mesh method was proposed in our research. The CPU time to generate an unstructured mesh was 0.14s compared with 0.05s of a locally modified mesh for a 32 by 32 mesh. To generate a 1024 by 1024 mesh, the CPU time of unstructured mesh was 8.65s compared with 0.56s of a locally modified mesh. For a complicated mesh generation problem, our method showed a significantly improvement on efficiency. In chapter 4, we demonstrated an augmented variable method to accurately compute the gradient along the boundary or the interface. Our result showed that there was a tradeoff between efficiency and accuracy. This method sacrificed some efficiency to obtain a higher level of accuracy by enlarging the stiffness matrix. Moreover, the stiffness matrix became a rectangular matrix which increases the challenges in solving it.

Thirdly, we designed algorithms. In this dissertation, different algorithms, such as domain decomposition algorithm and locally modified algorithm were built. Those methods were easy to follow and can be conveniently applied to other problems, such as systemx other than Stokes-Darcy interaction, PDEs with complicated interface and domain structure. Besides, those algorithms have been theoretically proved with elegant mathematical tools and thoughts which provides valuable ideas for future implementations.

In the end, we have identified several areas of future research goals from our results in this thesis.

First, for the accurate gradient computation method, we can design and test on different finite element spaces to check if a second order accuracy on the gradient can be obtained. Moreover, a theoretical proof of the convergence of this new method is highly desired.

Second, it is interesting to extend the locally modified mesh method to 3D. The mesh generation process of a 3D problem is even more complicated and time consuming. Using locally modified mesh method, we might potentially reduce the time cost significantly. More importantly, we always get a body fitted mesh which originally might be more difficult for 3D problems.

BIBLIOGRAPHY

[1] J. Adams, P. Swarztrauber, and R. Sweet. Fishpack: Efficient Fortran subprograms for the solution of separable elliptic partial differential equations. *National Center for Athmospheric Research*, 1999.

[2] M. Amara, D. Capatina, and L. Lizaik. Coupling of Darcy-Forchheimer and compressible Navier-Stokes equations with heat transfer. *SIAM Journal on Scientific Computing*, 31(2):1470–1499, 2009.

[3] T. Arbogast and D. S. Brunson. A computational method for approximating a Darcy-Stokes system governing a vuggy porous medium. *Computational geosciences*, 11(3):207–218, 2007.

[4] S. Badia and R. Codina. Unified stabilized finite element formulations for the Stokes and the Darcy problems. *SIAM journal on Numerical Analysis*, 47(3):1971–2000, 2009.

[5] T. Beale and A. Layton. On the accuracy of finite difference methods for elliptic problems with interfaces. *Communications in Applied Mathematics and Computational Science*, 1(1):91–119, 2007.

[6] G. S. Beavers and D. D. Joseph. Boundary conditions at a naturally permeable wall. *Journal of fluid mechanics*, 30(01):197–207, 1967.

[7] J. B. Bell, C. N. Dawson, and G. R. Shubin. An unsplit, higher order Godunov method for scalar conservation laws in multiple dimensions. *Journal of Computational Physics*, 74(1):1–24, 1988.

[8] C. Börgers. A triangulation algorithm for fast elliptic solvers based on domain imbedding. *SIAM journal on numerical analysis*, 27(5):1187–1196, 1990.

[9] E. Burman. Pressure projection stabilizations for Galerkin approximations of Stokes' and Darcy's problem. *Numerical Methods for Partial Differential Equations*, 24(1):127–143, 2008.

[10] E. Burman and P. Hansbo. Stabilized Crouzeix-Raviart element for the Darcy-Stokes problem. *Numerical Methods for Partial Differential Equations*, 21(5):986–997, 2005.

[11] E. Burman and P. Hansbo. A unified stabilized method for Stokes and Darcy equations. *Journal of Computational and Applied Mathematics*, 198(1):35–51, 2007.

[12] Z. Cai, C. Tong, P. S. Vassilevski, and C. Wang. Mixed finite element methods for incompressible flow: Stationary Stokes equations. *Numerical Methods for Partial Differential Equations*, 26(4):957–978, 2010.

[13] Z. Cai, X. Ye, and S. Zhang. Discontinuous Galerkin finite element methods for interface problems: A priori and a posteriori error estimations. *SIAM Journal on Numerical Analysis*, 49(5):1761–1787, 2011.

[14] Z. Cai and S. Zhang. Recovery-based error estimators for interface problems: mixed and nonconforming finite elements. *SIAM Journal on Numerical Analysis*, 48(1):30–52, 2010.

[15] Y. Cao, M. Gunzburger, X. He, and X. Wang. Robin-Robin domain decomposition methods for the steady-state Stokes-Darcy system with the Beavers-Joseph interface condition. *Numerische Mathematik*, 117(4):601–629, 2011.

[16] Y. Cao, M. Gunzburger, X. Hu, F. Hua, X. Wang, and W. Zhao. Finite element approximations for Stokes-Darcy flow with Beavers-Joseph interface conditions. *SIAM Journal on Numerical Analysis*, 47(6):4239–4256, 2010.

[17] Y. Cao, M. Gunzburger, F. Hua, X. Wang, et al. Coupled Stokes-Darcy model with Beavers-Joseph interface boundary condition. *Communications in Mathematical Sciences*, 8(1):1–25, 2010.

[18] J. C. Cavendish. Automatic triangulation of arbitrary planar domains for the finite element method. *International Journal for Numerical Methods in Engineering*, 8(4):679–696, 1974.

[19] A. Çeşmelioğlu and B. Riviere. Analysis of time-dependent Navier-Stokes flow coupled with Darcy flow. *Journal of Numerical Mathematics*, 16(4):249–280, 2008.

[20] N. Chen, M. Gunzburger, and X. Wang. Asymptotic analysis of the differences between the Stokes-Darcy system with different interface conditions and the Stokes-Brinkman system. *Journal of Mathematical Analysis and Applications*, 368(2):658–676, 2010.

[21] W. Chen, M. Gunzburger, F. Hua, and X. Wang. A parallel Robin-Robin domain decomposition method for the Stokes-Darcy system. *SIAM Journal on Numerical Analysis*, 49(3):1064–1084, 2011.

[22] K. T. Chu and M. Prodanovic. Level set method library (LSMLIB), 2008.

[23] H. Darcy. *Les fontaines publiques de la ville de Dijon: exposition et application...* Victor Dalmont, 1856.

[24] S. Deng, K. Ito, and Z. Li. Three-dimensional elliptic solvers for interface problems and applications. *Journal of Computational Physics*, 184(1):215–243, 2003.

[25] M. Discacciati. *Domain decomposition methods for the coupling of surface and groundwater flows*. PhD thesis, École Polytechnique Fédérale de Lausanne, 2004.

[26] M. Discacciati. Iterative methods for Stokes-Darcy coupling. In *Domain decomposition methods in science and engineering*, pages 563–570. Springer, 2005.

[27] M. Discacciati, E. Miglio, and A. Quarteroni. Mathematical and numerical models for coupling surface and groundwater flows. *Applied Numerical Mathematics*, 43(1):57–74, 2002.

[28] M. Discacciati and A. Quarteroni. Analysis of a domain decomposition method for the coupling of Stokes and Darcy equations. In *Numerical mathematics and advanced applications*, pages 3–20. Springer, 2003.

[29] M. Discacciati and A. Quarteroni. Convergence analysis of a subdomain iterative method for the finite element approximation of the coupling of Stokes and Darcy equations. *Computing and Visualization in Science*, 6(2-3):93–103, 2004.

[30] M. Discacciati, A. Quarteroni, and A. Valli. Robin-Robin domain decomposition methods for the Stokes-Darcy coupling. *SIAM Journal on Numerical Analysis*, 45(3):1246–1268, 2007.

[31] P. A. Domenico and F. W. Schwartz. *Physical and chemical hydrogeology*, volume 506. Wiley New York, 1998.

[32] N. T. Frink. Recent progress toward a three-dimensional unstructured Navier-Stokes flow solver. In *AIAA, Aerospace Sciences Meeting & Exhibit, 32 nd, Reno, NV*, 1994.

[33] J. Fukuda and J. Suhara. Automatic mesh generation for finite element analysis. *Advances in computational methods in structural mechanics and design*, 1972.

[34] V. Girault and B. Rivière. DG approximation of coupled Navier-Stokes and Darcy equations by Beaver-Joseph-Saffman interface condition. *SIAM Journal on Numerical Analysis*, 47(3):2052–2089, 2009.

[35] R. Glowinski, T.-W. Pan, and J. Periaux. A Lagrange multiplier/fictitious domain method for the numerical simulation of incompressible viscous flow around moving rigid bodies:(i) case where the rigid body motions are known a priori. *Comptes Rendus de l'Académie des Sciences-Series I-Mathematics*, 324(3):361–369, 1997.

[36] F. Hecht. New development in FreeFem++. *Journal of Numerical Mathematics*, 20(3-4):251–266, 2012.

[37] K. Ho-Le. Finite element mesh generation methods: a review and classification. *Computer-aided design*, 20(1):27–38, 1988.

[38] T. Y. Hou, Z. Li, S. Osher, and H. Zhao. A hybrid method for moving interface problems with application to the Hele-Shaw flow. *Journal of Computational Physics*, 134(2):236–252, 1997.

[39] F. N. Hua. *Modeling, analysis and simulation of the Stokes-Darcy system with Beavers-Joseph interface condition*. The Florida State University, 2009.

[40] H. Huang and Z. Li. Convergence analysis of the immersed interface method. *IMA Journal of Numerical Analysis*, 19(4):583–608, 1999.

[41] K. Ito, K. Kunisch, and Z. Li. Level-set function approach to an inverse interface problem. *Inverse problems*, 17(5):1225, 2001.

[42] K. Ito, M.-C. Lai, and Z. Li. A well-conditioned augmented system for solving Navier-Stokes equations in irregular domains. *Journal of Computational Physics*, 228(7):2616–2628, 2009.

[43] B. Jiang. A parallel domain decomposition method for coupling of surface and groundwater flows. *Computer Methods in Applied Mechanics and Engineering*, 198(9):947–957, 2009.

[44] I. Jones. Low Reynolds number flow past a porous spherical shell. In *Mathematical Proceedings of the Cambridge Philosophical Society*, volume 73, pages 231–238. Cambridge Univ Press, 1973.

[45] T. Karper, K.-A. Mardal, and R. Winther. Unified finite element discretizations of coupled Darcy-Stokes flow. *Numerical Methods for Partial Differential Equations*, 25(2):311–326, 2009.

[46] B. J. Kirby. *Micro-and nanoscale fluid mechanics: transport in microfluidic devices*. Cambridge University Press, 2010.

[47] A. Klute. Laboratory measurement of hydraulic conductivity of saturated soil. *Methods of Soil Analysis. Part 1. Physical and Mineralogical Properties, Including Statistics of Measurement and Sampling*, (methodsofsoilana):210–221, 1965.

[48] D. Kwak, J. L. Chang, S. P. Shanks, and S. R. Chakravarthy. A three-dimensional incompressible Navier-Stokes flow solver using primitive variables. *AIAA journal*, 24(3):390–396, 1986.

[49] W. J. Layton, F. Schieweck, and I. Yotov. Coupling fluid flow with porous media flow. *SIAM Journal on Numerical Analysis*, 40(6):2195–2218, 2002.

[50] W. J. Layton, F. Schieweck, and I. Yotov. Coupling fluid flow with porous media flow. *SIAM Journal on Numerical Analysis*, 40(6):2195–2218, 2002.

[51] R. J. LeVeque. *Finite difference methods for ordinary and partial differential equations: steady-state and time-dependent problems*, volume 98. Siam, 2007.

[52] R. J. Leveque and Z. Li. The immersed interface method for elliptic equations with discontinuous coefficients and singular sources. *SIAM Journal on Numerical Analysis*, 31(4):1019–1044, 1994.

[53] R. J. LeVeque and Z. Li. Immersed interface methods for Stokes flow with elastic boundaries or surface tension. *SIAM Journal on Scientific Computing*, 18(3):709–735, 1997.

[54] Q. Li, K. Xu, and S. Fu. A high-order gas-kinetic Navier–Stokes flow solver. *Journal of Computational Physics*, 229(19):6715–6731, 2010.

[55] Z. Li. *The immersed interface method a numerical approach for partial differential equations with interfaces*. PhD thesis, Citeseer, 1994.

[56] Z. Li. Immersed interface methods for moving interface problems. *Numerical Algorithms*, 14(4):269–293, 1997.

[57] Z. Li. A fast iterative algorithm for elliptic interface problems. *SIAM Journal on Numerical Analysis*, 35(1):230–254, 1998.

[58] Z. Li. An augmented cartesian grid method for stokes–darcy fluid–structure interactions. *International Journal for Numerical Methods in Engineering*, 2015.

[59] Z. Li and K. Ito. Maximum principle preserving schemes for interface problems with discontinuous coefficients. *SIAM Journal on Scientific Computing*, 23(1):339–361, 2001.

[60] Z. Li and K. Ito. *The immersed interface method: numerical solutions of PDEs involving interfaces and irregular domains*, volume 33. Siam, 2006.

[61] Z. Li, K. Ito, and M.-C. Lai. An augmented approach for Stokes equations with a discontinuous viscosity and singular forces. *Computers & Fluids*, 36(3):622–635, 2007.

[62] Z. Li and M.-C. Lai. The immersed interface method for the Navier-Stokes equations with singular forces. *Journal of Computational Physics*, 171(2):822–842, 2001.

[63] Z. Li, S. R. Lubkin, and X. Wan. An augmented IIM-level set method for Stokes equations with discontinuous viscosity. *Electron. J. Differential Equations*, 15:193–210, 2007.

[64] Z. Li and P. Song. An adaptive mesh refinement strategy for immersed boundary/interface methods. *Communications in computational physics*, 12(02):515–527, 2012.

[65] Z. Li and P. Song. Adaptive mesh refinement techniques for the immersed interface method applied to flow problems. *Computers & structures*, 122:249–258, 2013.

[66] Z. Li, H. Zhao, and H. Gao. A numerical study of electro-migration voiding by evolving level set functions on a fixed Cartesian grid. *Journal of Computational Physics*, 152(1):281–304, 1999.

[67] X.-D. Liu, R. P. Fedkiw, and M. Kang. A boundary condition capturing method for Poisson's equation on irregular domains. *Journal of computational Physics*, 160(1):151–178, 2000.

[68] X.-D. Liu and T. Sideris. Convergence of the ghost fluid method for elliptic equations with interfaces. *Mathematics of computation*, 72(244):1731–1746, 2003.

[69] K. A. Mardal, X.-C. Tai, and R. Winther. A robust finite element method for Darcy-Stokes flow. *SIAM Journal on Numerical Analysis*, 40(5):1605–1631, 2002.

[70] A. Mayo. The fast solution of Poisson's and the biharmonic equations on irregular regions. *SIAM Journal on Numerical Analysis*, 21(2):285–299, 1984.

[71] A. Mayo. A decomposition finite difference method for the fourth order accurate solution of Poisson's equation on general regions. *International Journal of High Speed Computing*, 3(02):89–106, 1991.

[72] A. Mayo. The rapid evaluation of volume integrals of potential theory on general regions. *Journal of Computational Physics*, 100(2):236–245, 1992.

[73] D. M. McQueen and C. S. Peskin. A three-dimensional computational method for blood flow in the heart. ii. Contractile fibers. *Journal of Computational Physics*, 82(2):289–297, 1989.

[74] A. Mikelic and W. Jäger. On the interface boundary condition of Beavers, Joseph, and Saffman. *SIAM Journal on Applied Mathematics*, 60(4):1111–1127, 2000.

[75] M. Mu and J. Xu. A two-grid method of a mixed Stokes-Darcy model for coupling fluid flow with porous media flow. *SIAM journal on numerical analysis*, 45(5):1801–1813, 2007.

[76] C. S. Peskin. Numerical analysis of blood flow in the heart. *Journal of computational physics*, 25(3):220–252, 1977.

[77] C. S. Peskin. Lectures on mathematical aspects of physiology. *Lectures in Appl. Math*, 19(69):107, 1981.

[78] C. S. Peskin and D. M. McQueen. A three-dimensional computational method for blood flow in the heart i. immersed elastic fibers in a viscous incompressible fluid. *Journal of Computational Physics*, 81(2):372–405, 1989.

[79] P. Popov, Y. Efendiev, and G. Qin. Multiscale modeling and simulations of flows in naturally fractured karst reservoirs. *Communications in computational physics*, 6(1):162, 2009.

[80] B. Riviére. Analysis of a discontinuous finite element method for the coupled Stokes and Darcy problems. *Journal of Scientific Computing*, 22(1):479–500, 2005.

[81] B. Rivière and I. Yotov. Locally conservative coupling of Stokes and Darcy flows. *SIAM Journal on Numerical Analysis*, 42(5):1959–1977, 2005.

[82] P. Saffman. On the boundary condition at the interface of a porous medium. *Stud. Appl. Math.*, 1:77–84, 1971.

[83] A. G. Salinger, R. Aris, and J. J. Derby. Finite element formulations for large-scale, coupled flows in adjacent porous and open fluid domains. *International Journal for Numerical Methods in Fluids*, 18(12):1185–1209, 1994.

[84] R. Shaw and R. Pitchen. Modification to the Suhara-Fukuda method of network generation. *International Journal for Numerical Methods in Engineering*, 12(1):93–99, 1978.

[85] G. Shubin and J. Bell. An analysis of the grid orientation effect in numerical simulation of miscible displacement. *Computer methods in applied mechanics and engineering*, 47(1):47–71, 1984.

[86] L. Song, Y. Hou, and Z. Cai. Recovery-based error estimator for stabilized finite element methods for the Stokes equation. *Computer Methods in Applied Mechanics and Engineering*, 272:1–16, 2014.

[87] B. Soni, Zhilin Li. Fast and accurate numerical approaches for Stefan problems and crystal growth. *Numerical Heat Transfer: Part B: Fundamentals*, 35(4):461–484, 1999.

[88] A. N. Tikhonov and A. A. Samarskii. Homogeneous difference schemes. *USSR Computational Mathematics and Mathematical Physics*, 1(1):5–67, 1962.

[89] S. Tlupova and R. Cortez. Boundary integral solutions of coupled Stokes and Darcy flows. *Journal of Computational Physics*, 228(1):158–179, 2009.

[90] X. Wan. *Numerical simulation methods for biological tissue interactions.* PhD thesis, North Carolina State University Libraries, 2006.

[91] Z. Wang. A quadtree-based adaptive Cartesian/Quad grid flow solver for Navier-Stokes equations. *Computers & Fluids*, 27(4):529–549, 1998.

[92] Z. Wang, Z. Li, and S. Lubkin. A Robin-Robin domain decomposition method for a Stokes-Darcy structure interaction with a locally modified mesh. *Numerical Mathematics: Theory, Methods & Applications*, 7(4), 2014.

[93] H. Xie, K. Ito, Z. Li, and J. Toivanen. A finite element method for interface problems with locally modified triangulation. *Contemporary Mathematics*, 466:179–190, 2008.

[94] X. Xie, J. Xu, and G. Xue. Uniformly-stable finite element methods for Darcy-Stokes-Brinkman models. *JOURNAL OF COMPUTATIONAL MATHEMATICS-INTERNATIONAL EDITION-*, 26(3):437, 2008.

[95] J.-J. Xu, Z. Li, J. Lowengrub, and H. Zhao. A level-set method for interfacial flows with surfactant. *Journal of Computational Physics*, 212(2):590–616, 2006.

[96] S. Zhang, X. Xie, and Y. Chen. Low order nonconforming rectangular finite element methods for Darcy-Stokes problems. *Journal of Computational Mathematics*, 27, 2009.